Space Flight Technology, German Space Operations Center (GSOC)
Deutsches Zentrum für Luft- und Raumfahrt (DLR) e.V.

Phoenix-S/-XNS Performance Validation

O. Montenbruck, C.Renaudie

Doc. No. : GTN-TST-0120
Version : 1.0
Date : Apr. 5, 2007

DLR

Document Change Record

Issue	Date	Pages	Description of Change
1.0	Apr. 5, 2007	All	First release

Table of Contents

Acronyms and Abbreviations

ADM	Atmospheric Dynamics Mission
C1	RINEX identifier for C/A code measurements (on L_1)
C/A	Coarse/Acqusition Code
C/N_0	Carrier-to-Noise ratio [dB-Hz]
D1	RINEX identifier for Doppler measurements on L_1
DLL	Delay-Locked Loop
DLR	Deutsches Zentrum für Luft- und Raumfahrt
DOP	Dilution Of Precision
FLL	Frequency-Locked Loop
GPS	Global Positioning System
GSOC	German Space Operations Center
IGS	International GNSS Service
L_1	GPS frequency (1575.42 MHz)
LA	RINEX identifier for carrier phase meas. On L_1 (C/A-code loop)
LEO	Low Earth Orbit
n/a	Not available, not applicable
NVM	Non-Volatile Memory
PDOP	Position Dilution of Precision
PLL	Phase-Locked Loop
POD	Precise Orbit Determination
ppm	Parts-Per-Million
PPS	Pulse-Per-Second
PRN	Pseudo-Random Noise
PVT	Position, Velocity, Time
R/F	Radio Frequency
RINEX	Receiver Independent Exchange Format
rms	Root Mean Square
RTC	Real-Time Clock
SGPS	Spaceborne GPS
SNR	Signal-to-Noise Ratio
TCXO	Temperature Controlled Oscillator
TEC	Total Electron Content
TECU	TEC unit ($10^{16e-}/m^2$)
TTFF	Time-To-First-Fix
UERE	User Equivalent Range Error
VTEC	Vertical Total Electron Content
XNS	eXtended Navigation System

Scope

This document provides an analysis of GPS data collected during the functional and performance testing of an engineering model of the Phoenix-S/-XNS receiver in a signal simulator testbed. The report covers the proper operation of the core tracking and positioning functions of as well as the eXtended Navigation System. It is applicable for receiver software versions D09B and up.

1. Introduction

1.1 Phoenix Receiver Description

The Phoenix GPS receiver ([1], [2]) is a miniature receiver specifically designed for high dynamics space applications. It is based on SigTech's commercial-off-the-shelf MG5001 receiver board but operates a proprietary firmware developed by DLR. Though originally designed for automotive applications, the receiver board has been qualified for space use in a series of thermal-vacuum, vibration and total ionization dose tests. The receiver employs a GP4020 baseband processor which combines a 12 channel GP2021 correlator and an ARM7TDMI microprocessor kernel. At a power consumption of less than one Watt and a board size of 50 x 70 mm the receiver is among the smallest of its kind and particularly well suited for satellites with limited onboard resources. The Phoenix receiver is extensively used in European sounding rocket missions and has been selected for various other micro-satellite missions in low Earth orbit (LEO) such as PROBA-2, X-Sat, ARGO, Flying Laptop and PRISMA.

Fig. 1.1 Phoenix GPS Receiver

For satellite applications, two different versions of the Phoenix receiver are available to cover different mission needs:

- The Phoenix-S receiver provides basic GPS tracking and navigation functions for LEO satellites . It offers a built-in orbit propagator to aid the initial acquisition and to allow a short time-to-first-fix. Low-noise code and carrier phase measurements are achieved through carefully optimized tracking loops. Full cycle integer ambiguities enable precision relative navigation in carrier phase differential GPS applications.
- The Phoenix-XNS extends the functionality of the basic receiver version by a built-in navigation filter for LEO satellites ([3], [4]). It offers a dynamically smoothed and continuous navigation solution even in case of limited GPS satellite visibility. The measurement processing inside the Phoenix-XNS provides a rigorous elimination of ionospheric path delays and enables a real-time navigation accuracy meeting the requirements of advanced remote sensing satellites.

The Phoenix-XNS receiver requires a larger memory but is otherwise compatible with the basic Phoenix-S model. All test results on the acquisition, tracking, and kinematic navigation performance provided that are provided later in this report are equally applicable for both versions.

Specific features of the Phoenix-S/-XNS receiver software for LEO applications include optimized tracking loops for high accuracy code and carrier tracking, precision timing and integer

ambiguities for carrier phase based relative navigation, a twoline elements orbit propagator for signal acquisition aiding, and an attitude interface to account for non-zenith pointing antennas in the channel allocation process. A pulse-per-second signal enables synchronization to GPS (or UTC) time with an accuracy of better than 1μs. Noise levels of 0.4 m (pseudo-range) and 0.5 mm (carrier phase) at representative signal conditions (C/N_0=45dB-Hz) have been demonstrated in signal simulator and open air tests which render the receiver suitable for precise orbit determination. While the instantaneous (kinematic) navigation solution is restricted to an accuracy of roughly 10m (3D rms) due to broadcast ephemeris errors and unaccounted ionospheric path delays, an accuracy of about 0.5-1m can be achieved in a ground based precise orbit determination.

1.2 Test Environment and Configuration

All tests described in this report have been conducted at DLR premises on various tests dates in 2006 using an engineering model of the Phoenix-XNS receiver. Artificial GPS signals for a user satellite in low Earth orbit were generated by a Spirent STR4500 signal simulator [5] providing L1 signals for up to 12 satellites.

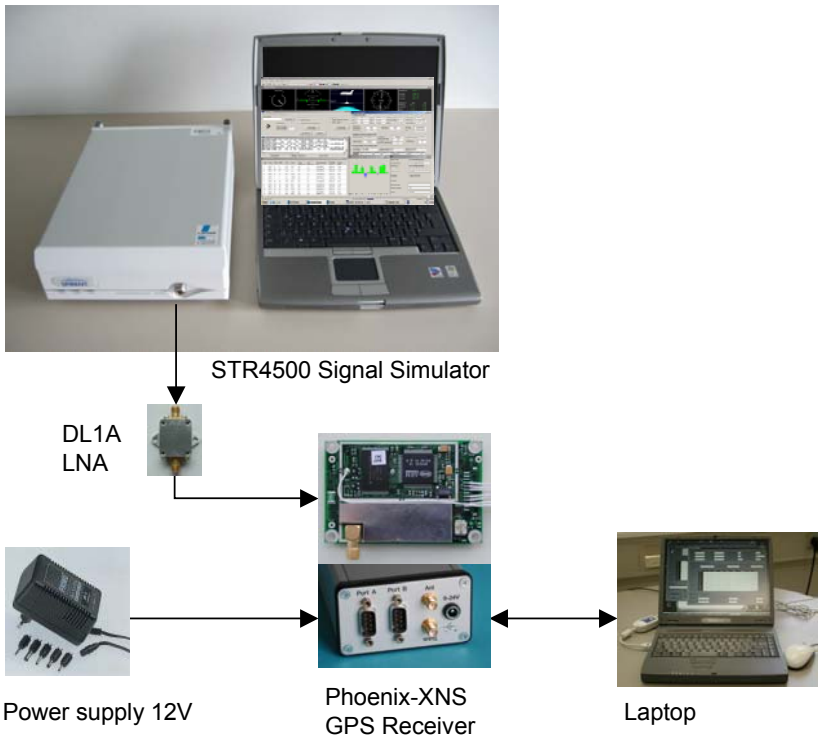

Fig 1.2 Test setup for Phoenix performance testing

The employed hardware components are summarized in Table 1.1. An overview of the test configuration is given in Fig. 1.2.

Table 1.1 Hard- and software configuration used in the Phoenix GPS receiver tests

Item	Description
Test receiver	Phoenix GPS receiver S/N 5 (512kB RAM) Software version D09B (ORBXNS) DL1A low noise amplifier S/N 2005004
Signal simulator	Spirent STR4500 unit #1617 12 channels L1 (C/A), default signal power setting +8dB SimPLEX for Windows v2-08 (patch 07/02/20) Scenarios created using SimGEN for Windows v2.53 on Spirent STR7790 unit #7033

The test scenario is based on a polar low Earth orbit and has previously been defined within the ADM-Aeolus project [6]. A detailed specification of the DLR_AEO scenario is provided in Chap. 2. For use with the STR4500 simulator, SimPLEX scenario files have first been generated on an STR7790 simulator using the SimGEN for Windows software.

1.3 Test Matrix

For a detailed assessment of the Phoenix GPS receiver performance and its response to various error sources, a total of four test runs with different parameter settings has been performed (Table 1.2).

Table 1.2 Test cases for Phoenix performance assessment.

Case	Ephemeris Errors	Simulated TEC	Duration	Rationale
A	off	0 TECU	24h	“Error free” case
B	on	0 TECU	24h	Assess impact of ephemeris errors
C	off	10 TECU	24h	Assess impact of ionospheric delays
D	on	10 TECU	24h	Overall performance assessment

1.4 Receiver Configuration

The employed configuration of the Phoenix receiver (ORBXNS) makes use of specific default settings and configuration parameters that control the receiver function and operation. Parameters that are of relevance for the execution of the signal simulator tests and the interpretation are summarized in Table 1.3.

Table 1.3 Default settings of the ORBXNS configuration for signal tracking, dynamical trajectory modeling, filtering and data handling.

Parameter	Value
Antenna line of sight vector	Zenith
Frame for antenna line of sight vector	n/a
Elevation mask	5°
Gravity model	GGM01
Gravity model degree and order	40
Mass	100 kg
Cross-section	1 m^2
C_R , C_D	1.3, 2.3
Pole coordinates (x_{pole},y_{pole})	0.0”, 0.0”
Standard deviation GRAPHIC data	0.25 m
Standard deviation of a priori position & velocity	100 m, 0.1 m/s
Standard deviation of C_R, C_D	0.1, 0.1
Std. dev. of a priori empirical acceleration in RTN direction	(100,200,200) 10^{-9} nm/s^2
Standard deviation of a priori clock offset	100 m
Standard deviation of a priori ambiguity	2 m
Autocorrelation time of empirical acceleration [s]	600 s
Steady state variance of empirical accelerations in RTN direction	(10,50,100) 10^{-9} nm/s^2
Autocorrelation time of clock offset	60 s
Steady state variance of clock offset	5 m

2. Aeolus Scenario Definition

The DLR_AEO scenario has originally been designed for GPS receiver performance testing in the context of the Aeolus mission [6]. The simulation is based on a Sun-synchronous, dusk-dawn orbit with 18h local time at the ascending node and a 390 km altitude. The epoch is chosen as 1 Oct. 2008, 0:00 GPS Time, and coincides with the descending node crossing. The GPS constellation is modeled based on the actual GPS almanac for week 1333, which is propagated to the scenario time within the signal simulator. To study the influence of ionospheric path delays and broadcast ephemeris errors different configuration files with optional error sources are provided. For parallel operation of the MosaicGNSS and Phoenix GPS receiver, a second antenna has been added to the DLR_AEO scenario. The antenna diagram is based on the measured pattern of a Seavey SPA-16C/S antenna.

2.1 Simulator Setup

The STR4760 simulator setup [7] is maintained in the form of hierarchical configuration files, each covering a specific group of parameters (cf. Table 2.1). All configuration data are stored in ASCII files using an XML format and can be modified using a standard text editor if required.

Table 2.1 Simulator configuration and output files for Phoenix receiver testing

File	Description
DLR_AEO.scn	Scenario root file
DLR_AEO_v1.veh	Vehicle specification
DLR_AEO_v1_a1.ant	Antenna specification
DLR_AEO_v1_a1_apc1.ant_pat_ctrl	Antenna switching control
DLR_AEO.ant_pat	Antenna pattern (Seavey SPA-16C/S)
DLR_AEO.aof	Antenna offsets (all zero)
DLR_AEO_v1_a1_rfl_mp1.rpatmp	Reflections (void)
DLR_AEO_v1_m1.mot	Vehicle motion specification
DLR_AEO.scr	Spacecraft reference (Aeolus orbit, 40x40 JGM3 model)
DLR_AEO.scm	Dummy s/c motion command file
DLR_AEO.scp	Spacecraft personality (C_D=2.3, mass=1300kg, A=8m^2)
DLR_PB2_v1_d1.aid	Aiding model specification (void)
DLR_AEO_tn_gps.net	GPS transmitter network specification
DLR_AEO_NoErr.gps	GPS constellation and signals (week1333 almanac, no clock & ephemeris errors, single-frequency, anti-spoofing bit set)
DLR_AEO_EphErr.gps	Same with supplementary ephemeris errors (UERE 1.5 m)
DLR_AEO_at1.atc	Atmosphere model specification
DLR_AEO_00TECU.atm	Troposphere and ionosphere (no TEC)
DLR_AEO_10TECU.atm	Same with constant VTEC 10 TECU
DLR_AEO.qlk	Quick-look data specification
ECEF_STATE_VEH1.qll	Quick-look logging specification (ECEF trajectory)
Yuma1333.txt	GPS Almanac in YUMA format for GPS week 1333 (=309+1024); used only upon creation of the GPS constellation definition (*.gps)
DLR_AEO_log.csv	Quick-look logging data in spreadsheet format
motion_V1.csv	Log file with motion data of user vehicle (orbit and attitude including derivatives) in spreadsheet format
satdata_V1A1.csv	Log files with simulated signal data (GPS position, pseudo-range and rate, atmospheric delays, etc.) for each channel in spreadsheet format

2.2 GPS Constellation

GPS Constellation

The GPS constellation definition stored in the *.gps configuration file is based on a YUMA almanac describing the true constellation for GPS week 1333 (=309) and reference epoch t_{oa}= 589824 s (i.e. approximately 16 months before the simulation epoch). It comprises a total of 29 satellites (all PRNs except 12, 17 and 32). For further reference a complete listing of the employed almanac file (Yuma1333.txt) is given in the Annex. The almanac file can be imported into a GPS constellation file using the “Load YUMA …” button of the Orbit Definition Window. It may be noted that PRN1 and PRN31 are simulated but have a non-nominal health code (“063” in the almanac file).

Ephemeris Errors

To assess the impact of broadcast ephemeris and clock errors on the navigation solution computed by the receiver, intentional position offsets have been added as part of the DLR_AEO_EphErr.gps configuration file. These offsets affect the simulated trajectory but are not applied to the broadcast ephemeris message issued by the simulator. The offsets are constant in time and applied only to the radial satellite position. No tangential and normal offsets have been configured since this would not provide added realism to the simulation. In an effort to mimic a realistic User Equivalent Range Error, the applied offsets are based on uniformly distributed random numbers with zero mean and a standard deviation of 1.5 m (cf. Table 2.2).

Table 2.2 Intentional broadcast ephemeris errors in downward direction (ΔZ) as applied in the DLR_AEO_EphErr.gps constellation definition file

PRN	Δr [m]	PRN	ΔZ [m]
1	-1.98	17	n.a.
2	0.87	18	1.26
3	-0.77	19	-0.46
4	0.07	20	1.67
5	-1.51	21	0.90
6	0.03	22	-0.88
7	-3.95	23	1.41
8	1.07	24	0.03
9	0.03	25	-0.38
10	-2.28	26	0.61
11	0.36	27	-0.53
12	n.a.	28	-2.65
13	1.38	29	-0.14
14	-2.65	30	0.36
15	1.80	31	1.87
16	1.06	32	n.a.

It is noted that the activation of broadcast ephemeris errors affects only the estimated receiver position but has virtually no impact on the velocity component of the navigation solution.

Satellite Selection

The simulator is configured to generate GPS signals for all satellites above a 5° obscuration angle measured from the Earth tangent. Satellites are selected based on a power level criterion using sequential replacement and 30s sampling. The actual elevation at which a specific satellite is selected or discarded depends on the total number of channels supported by the

simulator as well as the number of satellites visible at a specific time. Compared to a PDOP based channel allocation, the power level based selection ensures continuous and uninterrupted signals throughout the visibility period of each satellite. An appropriate entry is made in the Satellite Selection Page of the Constellation Editor.

GPS-UTC Difference

The GPS constellation file also specifies the difference between GPS and UTC time as part of the “General Control Details” menu. In accord with the expected offset for the considered epoch, a value of

GPS–UTC=14 s

has been adopted for the present simulation.

Signal Strength

By default, the simulator generates a GPS signal strength compatible with the minimum signal level specified for the GPS system in [8] (approx. –130 dBm for satellites at a mean distance from the observer) and a 0 dB vertical antenna gain. The overall signal level may, however, be adjusted to account for the actual antenna gain (ca. 3-5 dB in the boresight direction) as well as the actual GPS signal strength (approx. <3 dB above specification). In addition, a higher than normal signal level is required to compensate for the higher noise temperature experienced in simulator testing compared to the usual antenna sky temperature [9]. A software signal amplification of about +8 dB has therefore been recommended in [10] and found appropriate to reproduce the signal strengths observed in open-air receiver tests for various single-frequency GPS receivers.

This global amplification is configured in the Signal Control - Signal Power Page of the Constellation Editor. The antenna diagram itself is specified in the *.ant configuration file (cf. Sect. 2.5).

Clock and Ephemeris Errors

No intentional clock and ephemeris errors are applied in the DLR_AEO scenario.

Other General Control Details

In addition to the above parameters the following settings are chosen in the General Data Page:

Clock & Ephemeris Divergence	Disabled
Signal Strength	Modeled
Clock Noise	Disabled

Parameters not mentioned are of no significance for the conducted simulations.

Anti-Spoofing Flag

Since various receivers are known to distinguish between P code tracking and Y-code tracking based on the value of the Anti-Spoofing flag (bit 19 of the hand-over-word (HOW) in the GPS navigation message), it is advisable to ensure a consistent setting of this flag in the GPS constellation definition. To this end bit 19 of the hand-over-word (=word number 2) has been set to “1” for all simulated GPS satellites, subframes and pages in the Nav Data Modifications Window.

2.3 Atmospheric Characteristics

The application of ionospheric path delays (and a corresponding carrier phase advance) is controlled by the Atmosphere File Editor. The “Spacecraft” ionosphere model and a constant total electron content (TEC) are selected for the DLR_AEO scenario. To study the impact of varying ionospheric path delays, both a ionosphere free configuration (DLR_AEO_00TECU.atm) and a configuration with $1.0 \cdot 10^{17}$ electrons/m^2 = 10 TECU (DLR_AEO_10TECU.atm) are employed. Elevation dependent path delays in the simulator are modeled through the mapping function of Lear

The Klobuchar coefficients incorporated into the navigation message are specified in the Terrestrial Iono Data Window of the Atmosphere File. Values used in the simulation are summarized in Table 2.3. They are not designed to match the actually applied ionospheric path delay but may be used to check, whether ionospheric corrections are properly disabled in a spaceborne single frequency receiver.

Table 2.3 Klobuchar model coefficients for ionospheric refraction correction

Parameter	Value	Parameter	Value
α_0	$9.2 \cdot 10^{-9}$ s	β_0	87000 s
α_1	$1.8 \cdot 10^{-8}$ s/smc	β_1	50000 s/smc
α_2	$-7.2 \cdot 10^{-8}$ s/smc^2	β_2	-160000 s/smc^2
α_3	$-1.2 \cdot 10^{-7}$ s/smc^3	β_3	-330000 s/smc^3

2.4 Spacecraft Orbit and Attitude

The modeled spacecraft is assumed to fly in a near circular, polar orbit at 390 km altitude. In accord with the envisaged “dusk-dawn” configuration, the ascending node is located at 18^h local time. The epoch is chosen as 1 Oct. 2008, 0:00 GPS Time, and coincides with the descending node crossing. Adopted orbital elements (in the J2000 reference system) and the resulting ECEF epoch state vector are given in Table 2.4. The orbit is propagated by the simulator using a JGM-3 40 x 40 Earth gravity model as well as drag perturbations. The spacecraft orientation is specified as Earth-pointing with vanishing heading, elevation and bank angles in the orbital frame. Corresponding configuration data are specified in the spacecraft reference file (*.scr). Supplementary to the orbital parameters specified above, the spacecraft personality file (*.scp) specifies the ballistic properties of the satellite with assumed values of A=8 m^2, m=1300 kg, C_D=2.3.

Table 2.4 Simulated Aeolus spacecraft orbit

Epoch	2008 Sep 30, 23:59:46 UTC 2008 Oct 01, 00:00:00 GPS; GPS week 1499, 259200s				
Elements (J2000)	Value	State vector (ECEF)		Value	
Semi-major axis (a)	6768.0 km	Position	x	-8568.7529	m
Eccentricity (e)	0.0014		y	6774686.5220	m
Inclination (i)	97.0°		z	-14093.7802	m
Long. of ascend. node (Ω)	280.0°	Velocity	v_x	1434.9408258	m/s
Arg. of perigee (ω)	45.0°		v_y	-6.4318032	m/s
Mean anomaly (M)	135.0°		v_z	-7608.7369007	m/s

For initialisation of the Phoenix GPS reference receiver, the resulting trajectory has been adjusted to the SGP4 orbit model, which resulted in the set of NORAD twoline elements shown in Table 2.5.

Table 2.5 Twoline elements corresponding to the simulated spacecraft trajectory specified in Table 2.4

```
1 12345U 01999  A 08274.99984954 0.00009925  00000-0 011932-3 0    08
2 12345  97.0566 280.1276 0014617 355.8358 184.1688 15.61451002    03
```

The spacecraft motion file (*.scm) is nominally empty since no orbit and attitude maneuvers are considered in the scenario

A summary of the GPS satellite visibility resulting from the simulated user orbit and GPS constellation is shown in Figs. 2.2-2.3 for a two hours arc starting at the scenario epoch.

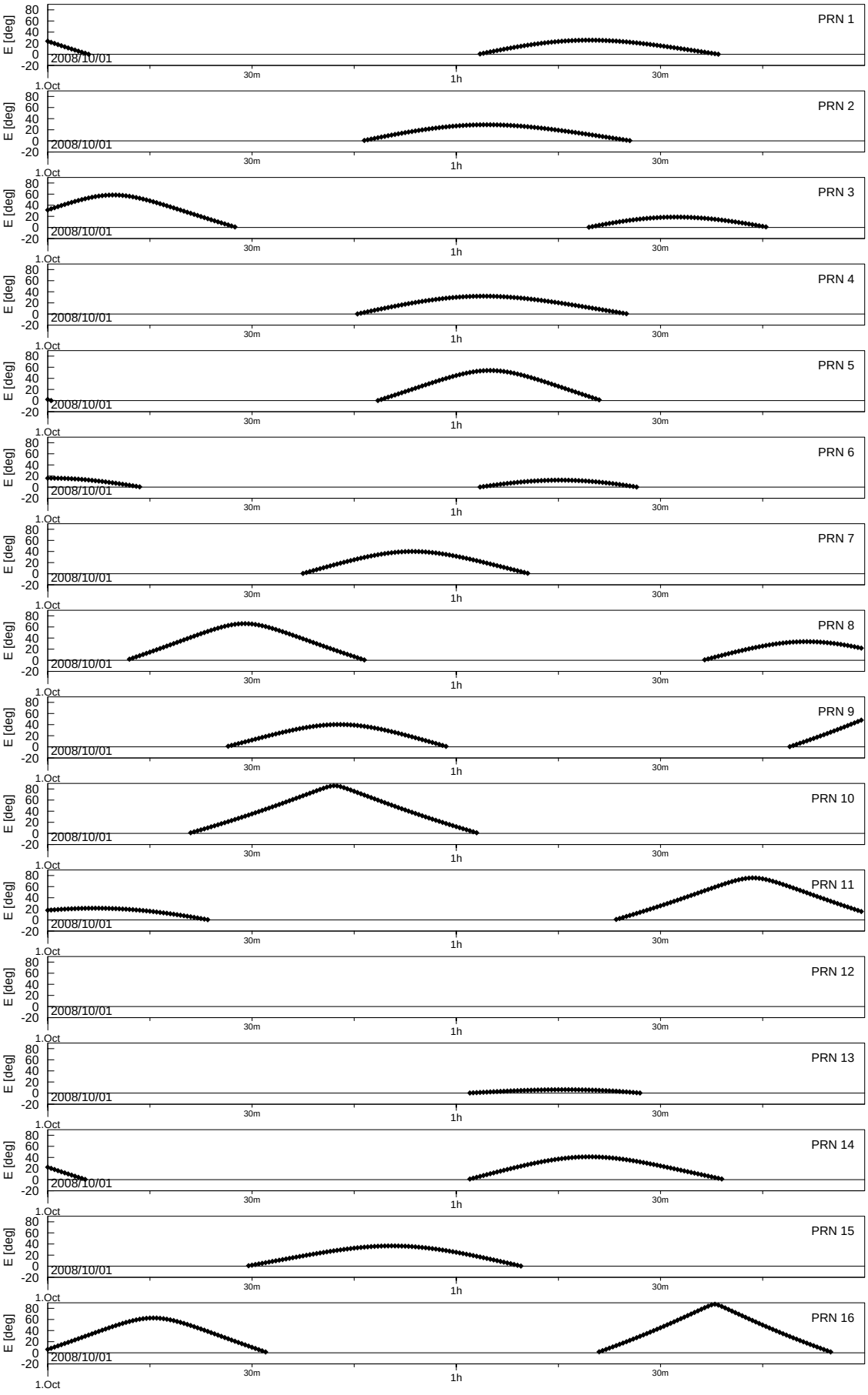

Fig 2.2 GPS satellite visibility in DLR_AEO scenario (PRN1-16)

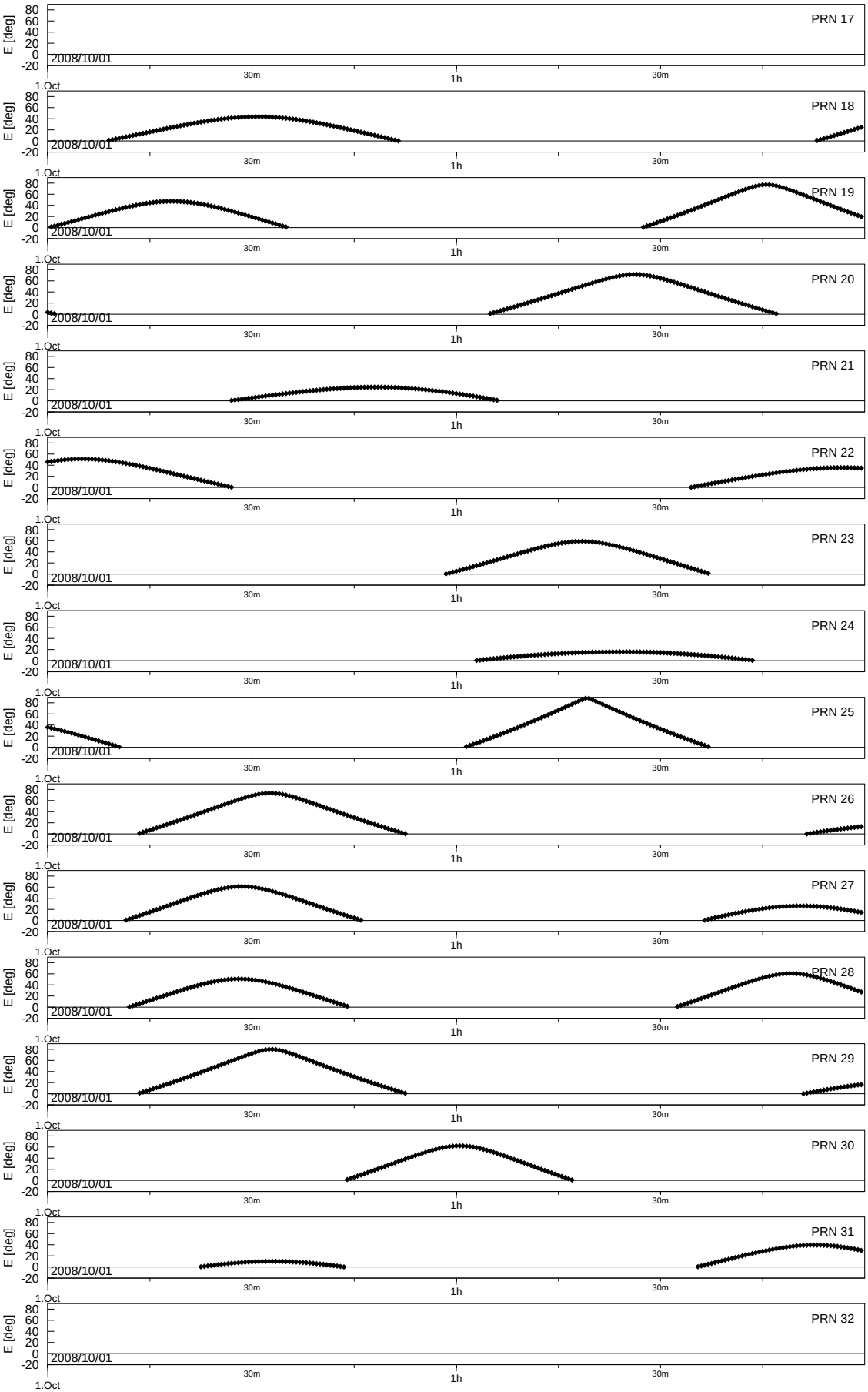

Fig 2.3 GPS satellite visibility in DLR_AEO scenario (PRN 17-32)

2.5 Antenna Diagram

The simulated gain pattern of the receiving antenna is based on the Seavey SPA-16C/S antenna employed by the MosaicGNSS receiver onboard Aeolus. Attenuation values relative to the vertical sensitivity are specified on a 5° elevation grid assuming an axis-symmetric antenna diagram (Table 2.6, Fig. 2.4). The employed gain values have been digitised by EADS Astrium based on gain patterns provided by the antenna manufacturer.

Table 2.6 SPA-16C/S antenna sensitivity pattern (gain loss relative to vertical gain)

E [°]	G [dB]	E [°]	G [dB]	E [°]	G [dB]	E [°]	G [dB]	E [°]	G [dB]
87 5	0 0	67 5	0 9	47 5	2 6	27 5	6 0	7 5	10 0
82 5	0 2	62 5	1 2	42 5	3 0	22 5	7 0	2 5	11 0
77 5	0 4	57 5	1 7	37 5	4 0	17 5	8 0	-2 5	12 0
72 5	0 7	52 5	2 1	32 5	5 0	12 5	9 0	-7 5	13 0

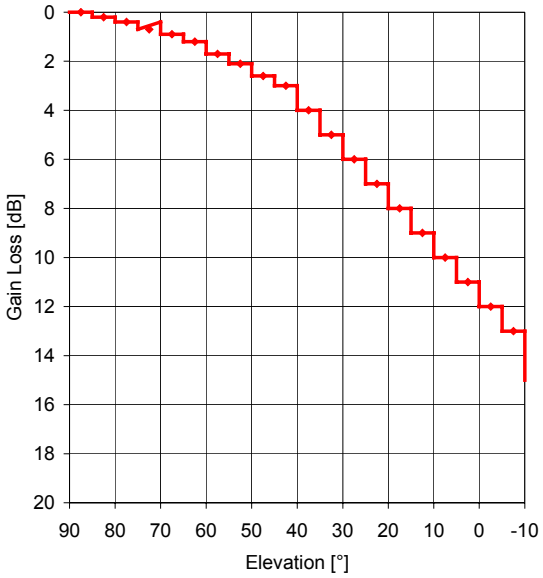

Fig 2.4 Antenna gain pattern of the Seavey SPA-16C/S antenna.

3. Acquisition Performance

3.1 Cold Start Acquisition

The Phoenix GPS receiver is designed to support a hot or warm start in low Earth orbit using a built-in orbit propagator, real-time clock (RTC) and non-volatile memory (NVM). Use of this functionality requires the activation of a keep alive-line, which may not be available in some missions or mission phases. In the absence of a priori information on the current time, orbit and GPS constellation, the receiver performs a cold start at power-up. Here, the receiver systematically checks all possible PRN codes and attempts a correlation in consecutive Doppler bins of 500 Hz widths. Within a given bin, the receiver takes roughly two seconds to scan all possible code offsets in 1/2 chip steps. Compared to a terrestrial environment, the Doppler shift experienced in a low Earth orbit may be roughly ten times larger (approx. ±45 kHz), which results in a notable increase of the cold start acquisition time.

Tests of the Phoenix GPS cold start acquisition performance have been conducted in an automated test bed, in which the test receiver was controlled by a Matlab/Simulink executive on the host PC [11]. During execution of the DLR_AEO scenario, F40 and F62 messages from the Phoenix output port were continuously monitored and recorded by this executive. Once a navigation solution had been achieved, a cold start (CS) command was issued after a configurable wait period of 1 to 3 min. In this way, a statistically representative number of cold starts (approx. 100 per day) with good orbital coverage could be collected in a single 24h signal simulator run with minimum operator intervention.

Dedicated builds of the Phoenix firmware were used to assess the impact of different Doppler search windows (11.5 kHz, 20 kHz, and 30 kHz) and to inhibit NVM support in the cold start test s with the Phoenix engineering model. Standard values were employed for the PDOP mask (10) and the elevation mask (5°).

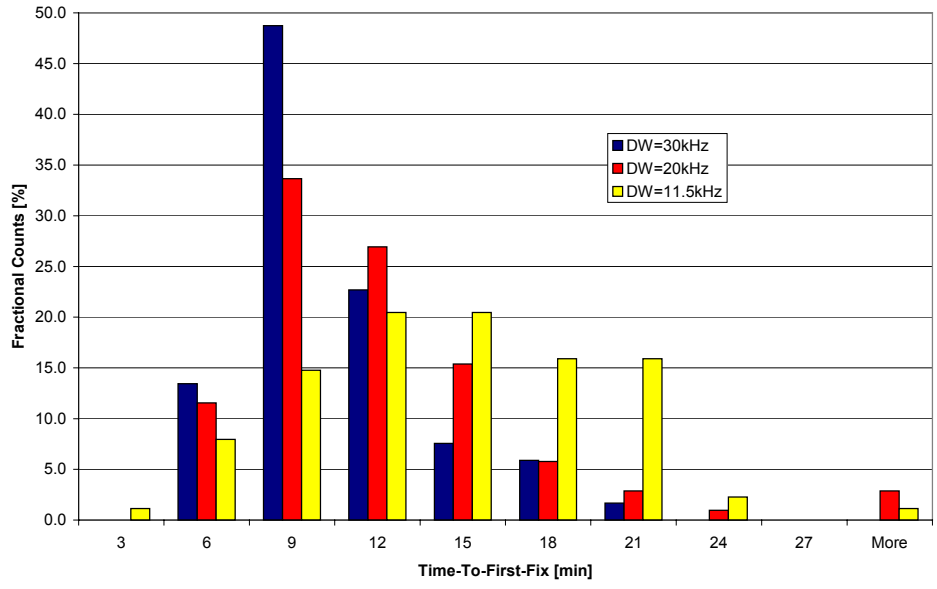

Fig 3.1 Distribution of Phoenix GPS cold times in the DLR_AEO scenario for different Doppler search windows (PDOP mask 10, elevation mask 5°).

For a search window of 30 kHz an average time-to-first-fix (TTFF) of 9 min was obtained and the cold start TTFF was less than 15 min In 92% of all samples. A slightly inferior performance was obtained for Doppler search windows of 20 kHz and 11.5 kHz, for which the average TTFF increased to 10.5 min and 13 min, respectively. In these cases the probability of achieving a navigation solution within less than 15 min amounted to 88% and 65%.

Based on the test results, a Doppler window of 30 kHz is recommended for an optimum cold start acquisition of the Phoenix GPS receiver. While smaller search windows result in an obvious degradation of the overall acquisition performance, a reliable acquisition and acceptable TTFF is even obtained with Doppler windows down to 10 kHz. The results clearly indicate that it is not necessary to extend the search window to the actual range of Doppler shifts (approx. 45 KHz) experienced by a GPS receiver onboard a LEO satellite. Instead, a smaller window results in more frequent reallocations of the available channels. This, in turn, increase the probability of acquiring a sufficiently large number of satellites with high elevation and low Doppler shift.

3.2 Hot Start Acquisition

The hot start capability of the Phoenix receiver has been assessed through a series of resets conducted at regular intervals for a two hours arc of the Aeolus scenario. The employed receiver unit was equipped with a backup battery to maintain the real-time clock as well as almanac, ephemeris and orbit data. On average the TTFF amounts to roughly 25s with a scatter of ±5s (Fig. 3.2).

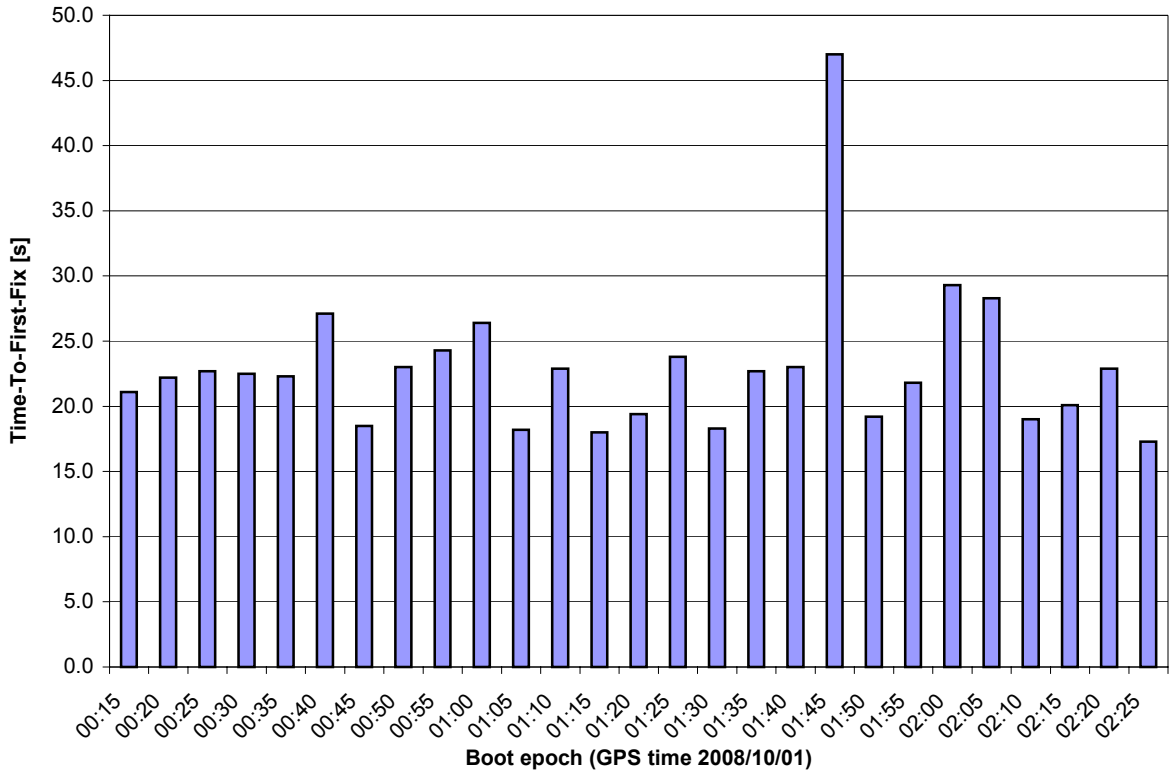

Fig 3.2 Hot-start time-to-first-fix of Phoenix GPS in the DLR_AEO scenario.

If current ephemeris parameters are not available (warm start condition), the respective data have to be extracted from the navigation data stream, first. At a subframe length of 30s, the download of an entire ephemeris data set for a specific channel may take up to 60s after a reboot to. The warm start time-to-first-fix may thus amount to 1-2 min.

4. Tracking Performance

4.1 Carrier-to-Noise Density

The discretization of the simulated antenna diagram (cf. Sect. 2.5) results in a stepwise variation of the carrier-to-noise density (C/N_0 in [db-Hz]) with the elevation of the simulated GPS satellites. This is illustrated in Fig. 4.1 for a 24 h arc of the DLR_AEO scenario with measurements sampled at 10 s intervals.

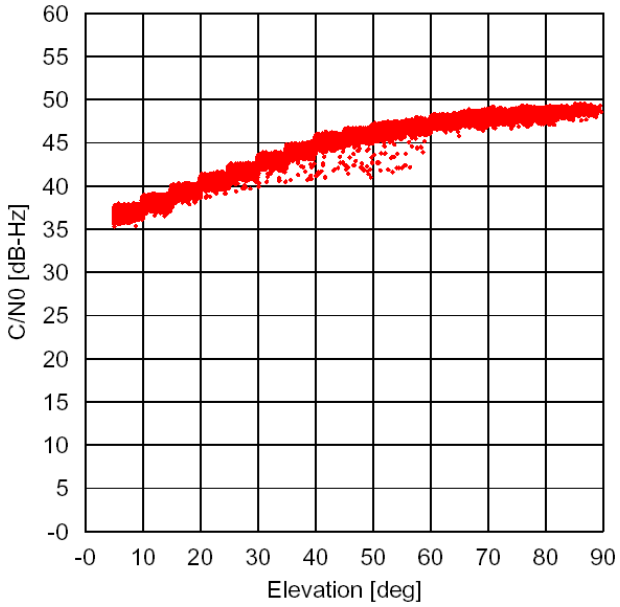

Fig 4.1 Relation between carrier-to-noise-density ratio and elevation of the GPS satellites for the Phoenix GPS receiver with DL1A preamplifier (DLR_AEO scenario with Seavey SPA-16C/S antenna, and +8dB signal power).

Peak C/N_0 values obtained in the test configuration amount to 49 dB-Hz, which roughly matches signal conditions encountered in open-air tests with the same LNA and a passive patch antenna. For the adopted antenna diagram and simulation scenario, the tracking is only limited by the pre-configured elevation mask of 5 deg. Minimum C/N_0 values of 37 dBHz at the elevation limit are still well above the tracking and acquisition threshold of the receiver.

4.2 Channel Allocation

The Phoenix GPS receiver provides a smooth and highly symmetric distribution of tracked satellites in the plane-of-sky (Fig. 4.2). An average of 10 GPS satellites is tracked in the DLR_AEO scenario and the full set of 12 tracking channels can occasionally be utilized. Satellites are properly released below the configured elevation mask of 5°. In the forward direction, the acquisition of new satellites takes place at about 8° elevation, which corresponds to a delay of roughly one minute relative to the theoretical acquisition time. This delay can in part be attributed to the update cycle of the cannel allocation algorithm and the required settling time of the tracking loops (10 seconds after frame lock) that is imposed by the receiver internal measurements screening.

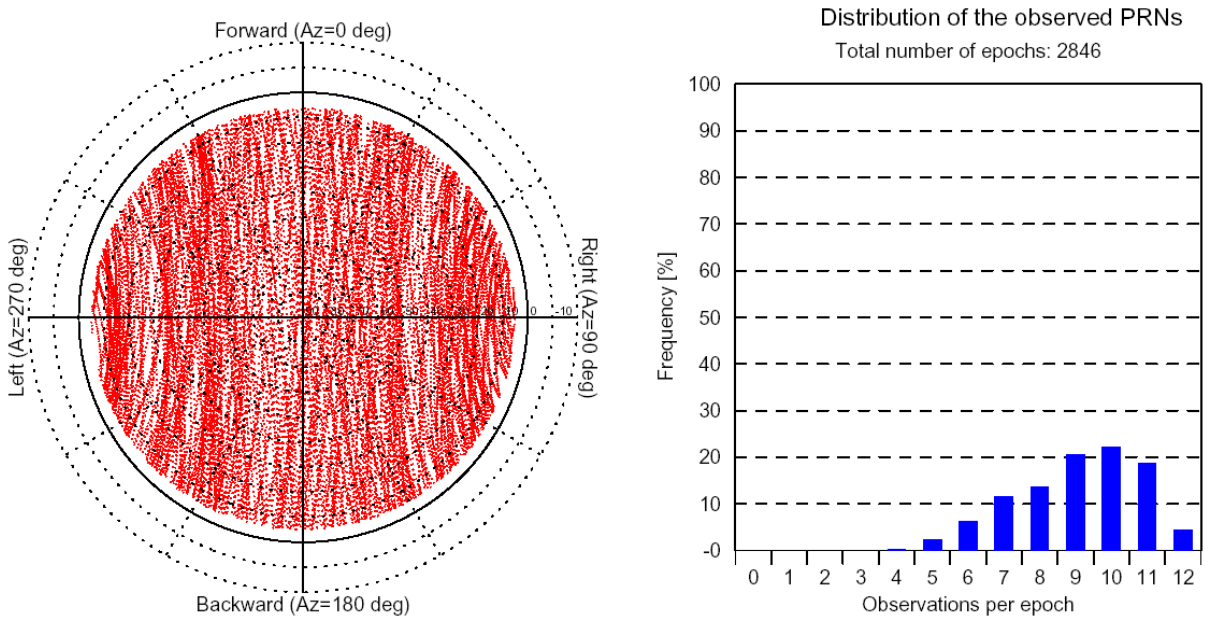

Fig 4.2 Skyplot and statistical distribution of tracked GPS satellites for a 24 hours arc using the DLR_AEO scenario.

4.3 Raw Measurement Accuracy

The raw measurement accuracy of the Phoenix receiver has been assessed using two variants of a zero-baseline test.

1. In the first test concept (“virtual zero-baseline test”; cf. [13]), double differences are formed from two sets of measurements collected in consecutive signal simulator runs with the same test scenario.
2. In the second variant (cf. [10]), double differences are formed against simulator truth values to assess the receiver noise as well as systematic errors.

Both concepts require only a single receiver unit, which is particularly useful in view of the high cost and limited availability of spaceborne GPS receivers:

In a traditional zero-baseline test, double-differences ($\nabla\Delta$) of code and phase measurements ρ from two receivers and two commonly observed GPS satellites are formed. For receivers connected to the same signal source, the result no longer depends on the geometric distance, clock errors and atmospheric path delays, but only on the receiver internal measurement noise ε. By selecting satellite pairs with closely matching C/N_0 (typically less than 1 dB-Hz) the noise of each individual measurement can be assumed to exhibit the same standard deviation, which is then obtained from

$$\sigma(\varepsilon) = \sigma(\nabla\Delta\rho)/\sqrt{4} \quad .$$

When working with a properly calibrated GPS signal simulator, the zero-baseline test can alternatively be conducted with data sets collected by a single receiver in two consecutive simulator runs. Since the same models are applied in the signal generation during repeated simulations, the signals differ only by noise originating from the simulator’s internal reference frequency. This noise contribution is identical for all simulator channels and therefore cancels upon forming double differences.

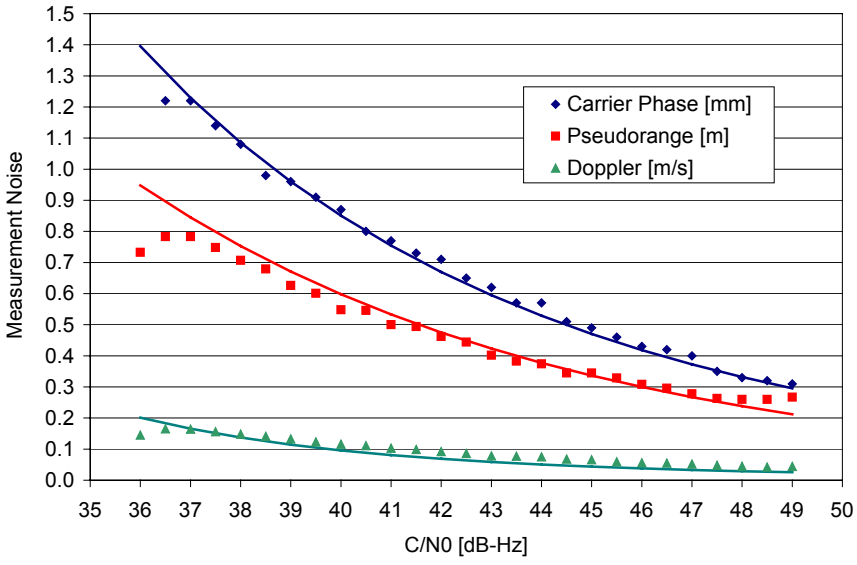

Fig. 4.3 Phoenix receiver noise versus carrier-to-noise-density-ratio

Using data collected in two 24h runs with the DLR_AEO scenario, the raw measurement noise of the Phoenix GPS receiver has been determined in 0.5 dBHz bins of C/N_0. The results shown in Fig. 4.3 for the pseudorange, carrier phase and Doppler measurements are consistent with DLL and PLL bandwidths of 1/12 Hz and 8 Hz, respectively (cf. [14]).

For a supplementary analysis of the receiver noise and systematic errors the SGPS performance test procedure introduced in [10] is employed. The analysis is based on double-differences between observed and simulated data on selected PRN pairs. After collecting the raw measurements over a two hour data arc, modeled pseudoranges and range rates are computed based on the simulated spacecraft trajectory and the known GPS constellation almanac. These are subtracted from the measurements to remove the varying geometry between the receiver and the GPS satellites from the data (cf. Fig. 4.4).

The result is essentially the sum of receiver clock errors (δt, δf), as well as measurement noise and tracking loop related errors (ε_i). To further eliminate the dominating clock terms, differences of two channels (A & B) are subsequently formed. Ideally, this results in a zero mean, white noise sequence with a variance equal to the sum of the noise variance of the individual channels. For two channels with similar signal-to-noise (SNR) ratios, the noise errors are expected to be of equal size and the r.m.s noise of the inter-channel difference is just $\sqrt{2}$ times as large as that of the undifferenced measurements. Other than in a zero-baseline test, only one receiver is required and systematic errors (related to e.g. the signal dynamics) can be revealed instead of being cancelled between receivers.

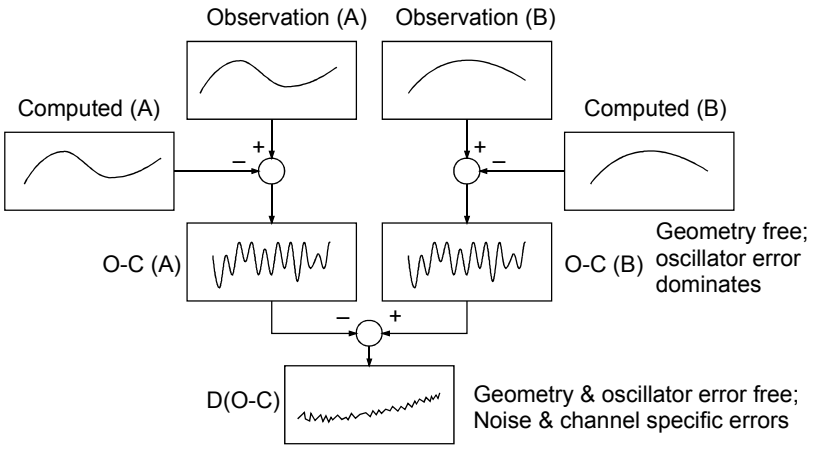

Fig. 4.4 Data analysis concept for assessment of raw data quality from measured and simulated pseudorange and carrier phase data

Results of the raw data analysis are collated in Table 4.1 for a set of data arcs and GPS satellite pairs with common (set 1-3) and overlapping (set 4-6) visibility. In addition to raw pseudorange, carrier phase and Doppler measurements, the noise characteristics of carrier-phase smoothed pseudoranges and range rates based on time differenced carrier phases are given. For illustration, sample plots of double differences between individual channels are, furthermore, shown in Figs. 4.5 - 4.7. All values are based on a simulation without ionospheric path delays. Due to code-carrier divergence, systematic biases may be show up in carrier-phase smoothed pseudoranges in the presence of ionospheric delays.

On average over a full visibility period, the C/A-code measurements are typically accurate to 0.5 m, while the carrier phase measurements have representative noise levels of 0.8 mm. The Doppler-based range-rate measurements are accurate to roughly 10 cm/s, while range-rates based on time-differenced carrier phase measurements achieve an accuracy of about 2 cm/s. This is consistent with the expected noise level of

$$\sigma(\dot{\rho}) = \sqrt{13}\sigma(\rho_{L1}) / 0.1\text{s}$$

for a quadratic fit of carrier phases over 0.1s time intervals [15].

Table 4.1 Standard deviation of Phoenix raw data obtained for the DLR_AEO scenario at a global signal power level of +8 dB. The individual data types are labeled by their RINEX identifiers (C1=pseudorange; LA=carrier phase, DA=Doppler; cf. [16]). The columns labelled C1* and DA* provide the noise characteristics of the smoothed pseudoranges and time differenced carrier phases, which are used for the internal navigation solution and output in the F41 message of the Phoenix receiver.

Set	PRN	Interval	Tracked	C1	C1*	LA	DA	DA*
1	26–29	[260000s,262400s]	[260107s, 262265s]	0.48 m	0.10 m	0.67 mm	0.090 m/s	0.016 m/s
2	27–28	[260000s,262400s]	[260023s, 261784s]	0.46 m	0.08 m	0.66 mm	0.093 m/s	0.016 m/S
3	..2– 4	[262000s,264200s]	[262123s, 264156s]	0.64 m	0.07 m	0.88 mm	0.120 m/s	0.020 m/s
4	..8–10	[260500s,262000s]	[260569s, 261920s]	0.45 m	0.09 m	0.72 mm	0.091 m/s	0.015 m/s
5	16–25	[264100s,265000s]	[264120s, 264958s]	0.46 m	0.10 m	0.90 mm	0.101 m/s	0.018 m/s
6	19–20	[264400s,265600s]	[264522s, 265536s]	0.45 m	0.06 m	0.83 mm	0.095 m/s	0.017 m/s

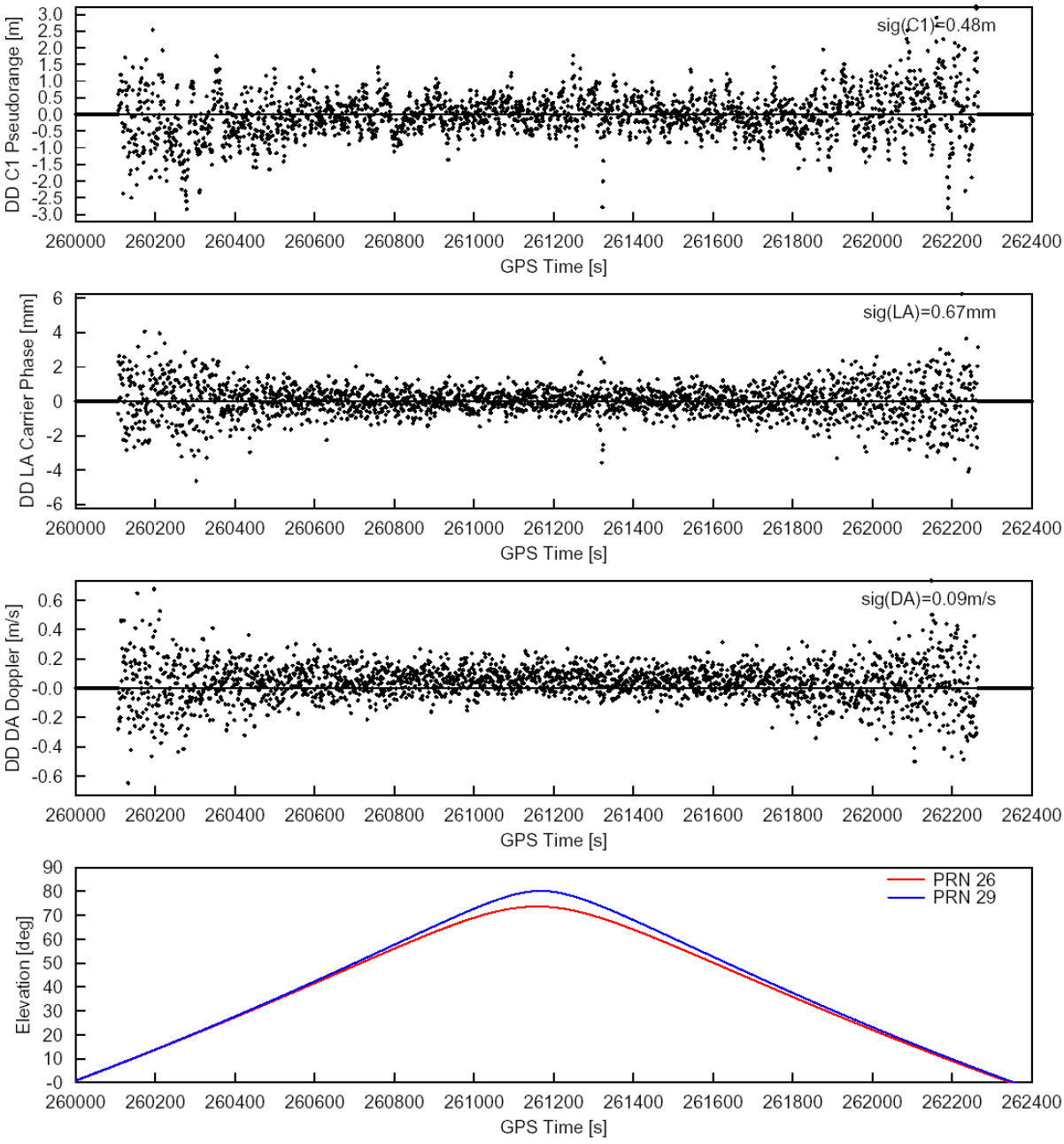

Fig. 4.5 Sample set of double differences (PRN 26-29, observed-modeled) of Phoenix GPS measurements (C1=pseudorange, LA=carrier phase, DA=Doppler) for common visibility

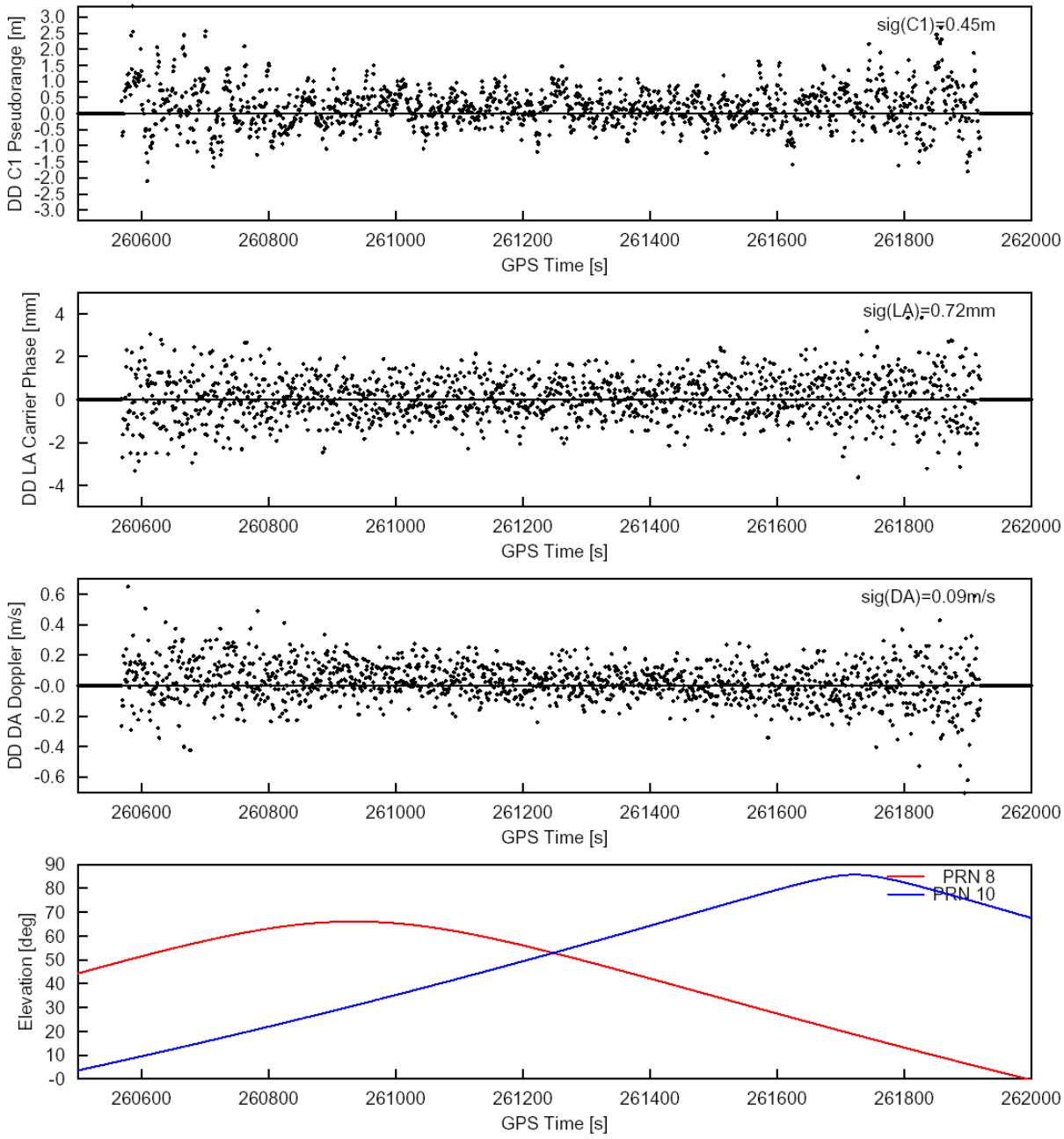

Fig. 4.6 Sample set of double differences (PRN 8-10, observed-modeled) of Phoenix GPS measurements (C1=pseudorange, LA=carrier phase, DA=Doppler) for overlapping visibility

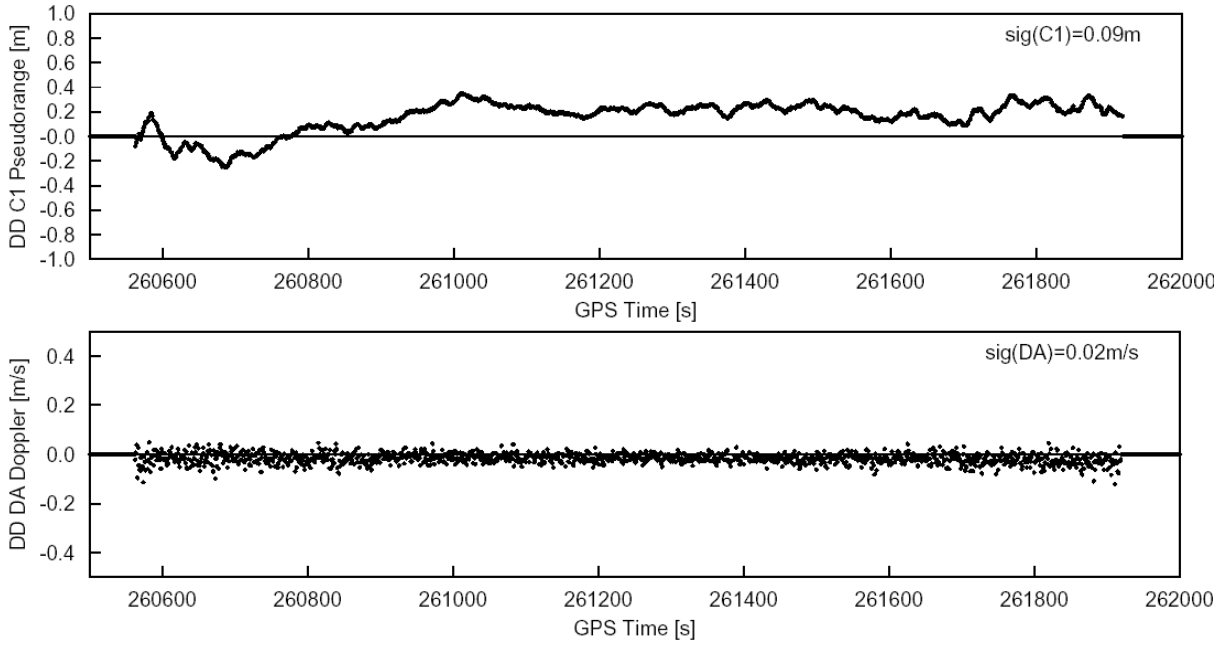

Fig. 4.7 Double differences of carrier-phase smoothed pseudoranges (C1) and range-rates from time differenced carrier phases (DA) for the PRN 8-10 pair (cf. Fig. 4.6)

5. Timing Performance

5.1 Oscillator Drift

The Phoenix GPS receiver employs a commercial temperature compensated crystal oscillator (TCXO) with a representative accuracy of 1.5 ppm. This corresponds to a frequency offset of up to 2.2kHz at the L1 frequency. At room temperature the actual oscillator error is generally much lower as indicated in Fig. 5.1. for a one day signal simulator test using the error free DLR_AEO scenario.

The oscillator error is determined as part of the kinematic navigation and reported in the F48 message of the Phoenix receiver. In accord with the velocity solution accuracy of about 5 cm/s, the individual oscillator offset values exhibit a scatter of less than 1Hz.

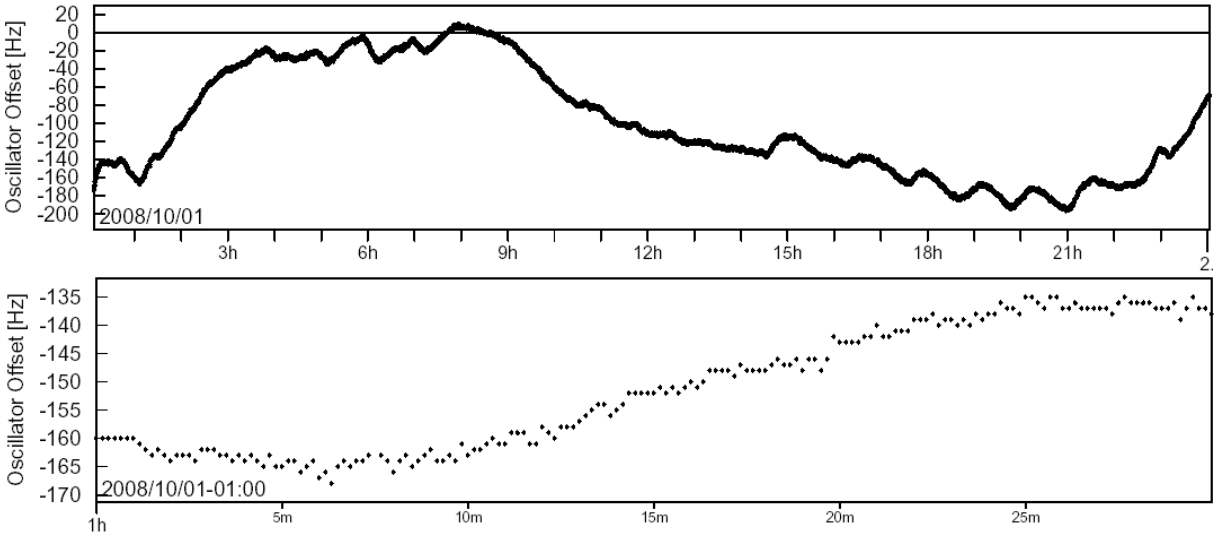

Fig. 5.1 Oscillator error as reported in the Phoenix F48 message for a one day signal simulator test (*top*) using the error-free DLR_AEO scenario. The lower figure shows a magnified view for a 30min slice.

It must be noted that the performance figures given above are only representative for the behavior of the Phoenix receiver during laboratory testing. Different performance characteristics may be obtained under exposure to thermal-vacuum conditions.

5.2 Pulse-Per-Second Signal

The ascending edge of the pulse-per-second signal generated by the Phoenix receiver is nominally aligned to integer second. Due to a 175ns discretization of the PPS timing, the actual instant of the PPS exhibits a typical scatter of ±0.1μs about the nominal value. This is illustrated in Fig. 5.2 based on a signal simulator test using an error free version of the DLR_AEO scenario. Additional, systematic shifts of the PPS may occur in the presence of uncorrected ionospheric path delays or broadcast ephemeris errors. In accord with the kinematic navigation solution accuracy these biases are likewise limited to less than ±0.1μs. The PPS signal is therefore typically accurate to ±0.2μs.

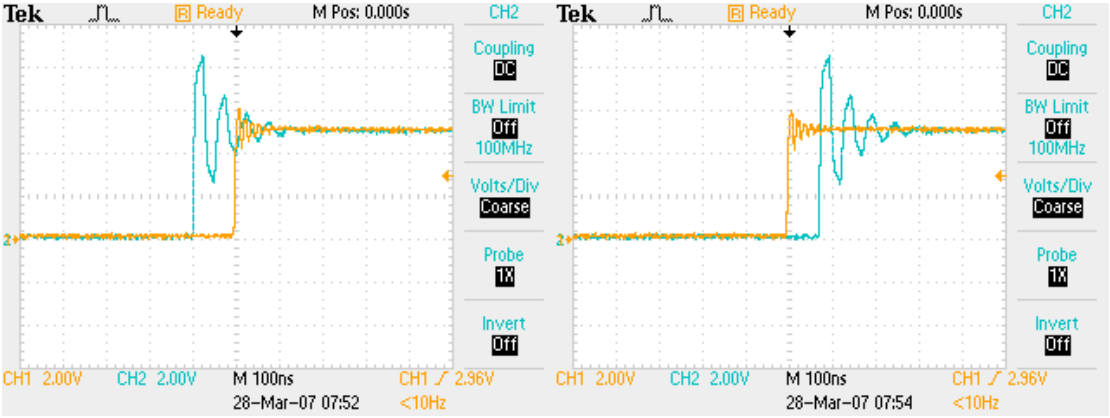

Fig. 4.2 Timing of the pulse-per-second signal (*blue*) relative to the true integer GPS second (*yellow*) as measured in a signal simulator test (DLR_AEO scenario) without broadcast ephemeris errors and ionospheric errors. Distortions of the PPS signal are due to improper impedance matching in the employed test setup and do not represent the actual pulse shape.

6. Navigation Performance

The navigation performance of the Phoenix receiver has independently been assessed for the kinematic navigation solution available in both the of the Phoenix-S and Phoenix-XNS as well as the dynamically filtered Phoenix-XNS navigation solution. Furthermore, the precise orbit determination accuracy achievable in a ground processing of raw tracking data is discussed. In accord with the test matrix defined in Sect. 1.3, independent tests have been conducted with and without broadcast ephemeris errors and with and without ionospheric errors to assess the respective contribution to the overall navigation accuracy.

6.1 Kinematic Navigation Accuracy

Results for the kinematic position and velocity solution for the various test cases are summarized in Tables 6.1a & b. In the error-free scenario (Case A), a 3D accuracy of 0.3-0.4 cm is achieved, which is dominated by a systematic along-track bias of about 0.3m. Similar errors have first been identified in the GPS Orion receiver and are most likely related to limitations of the employed frontend design. The bias varies among receiver units and is possibly altered by thermal-cycling. Furthermore, the bias is known to increase in inverse proportions to the bandwidth of the delay-locked loop [17].

The statistical errors of the kinematic navigation solution in the error-free scenario amount to roughly 0.25m and reflect the accuracy of the carrier phase smoothed pseudorange (approx. 0.1m) as well as the average dilution of precision in the horizontal and vertical direction. Likewise, the position errors are determined by the dilution of precision (along-track DOP ~1, cross-track DOP ~0.8, radial DOP ~2) and the simulated signal-in-space range error (1.5 m rms) when activating the broadcast ephemeris errors in Case B. Here the total position error amounts to roughly 4 m. A graphical representation of the individual errors is provided in Fig. 6.1a.

Table 6.1a Kinematic position solution accuracy of the Phoenix-S/XNS GPS receiver in the Aeolus test scenario

Case	Ephem. Errors	Iono. Errors	Arc	Radial [m]	Along-track [m]	Cross-track [m]	Position (3D rms)	Note
A	none	none	24h	+0.01 ± 0.25	+0.23 ± 0.11	+0.00 ± 0.09	0.37 m	#05, 070328
B	1.5m rms	none	24h	-0.33 ± 3.30	-0.00 ± 1.40	+0.09 ± 1.21	3.79 m	#05, 070402
C	none	10 TECU	24h	+6.37 ± 1.60	-1.61 ± 0.63	-0.02 ± 0.50	6.81 m	#05, 070329
D	1.5m rms	10 TECU	24h	+6.03 ± 3.79	-1.85 ± 1.51	+0.08 ± 1.35	7.63 m	#05, 070403

Table 6.1b Kinematic velocity solution accuracy of the Phoenix-S/XNS GPS receiver in the Aeolus test scenario

Case	Ephem. Errors	Iono. Errors	Arc	Radial [m/s]	Along-track [m/s]	Cross-track [m/s]	Velocity (3D rms)	Note
A	none	none	2h	+0.006±0.039	-0.000±0.019	+0.000±0.014	0.046 m/s	#05, 070328
B	1.5m rms	none	24h	+0.008±0.038	+0.000±0.018	+0.000±0.015	0.045m/s	#05, 070402
C	none	10 TECU	24h	+0.005±0.040	-0.014±0.019	-0.000±0.015	0.048m/s	#05, 070329
D	1.5m rms	10 TECU	24h	+0.005±0.041	-0.013±0.019	-0.000±0.015	0.050m/s	#05, 070403

The presence of uncorrected ionospheric path delays in Case C results in a mean shift of the radial position solution in proportion to the vertical delay. At a constant VTEC of 10 TECU, the vertical delay amounts to 1.6 m at the L1 frequency. This results in a radial bias of about 6 m, which is good accord with the analytical approximation derived in [18] for the Lear mapping function (cf. [11]) of the Spirent signal simulator and a 5° elevation mask. It may also be noted that an along-track bias of -1.8m shows up as a result of the ionospheric path delays. This bias can be attributed to the use of carrier-phase smoothed pseudoranges in the computation of the Phoenix navigation solution. At a smoothing interval of roughly 100s the smoothed ranges and thus the navigation solution are susceptible to the code-carrier diver-

gence, which then causes an apparent latency of the position solution. Single point solutions computed from offline from unsmoothed pseudoranges do not exhibit a VTEC dependent bias.

Upon combining broadcast ephemeris errors and ionospheric path delays (Test Case D), a 3D position error of about 8 m is obtained, which is again dominated by the radial offset (cf. Fig. 6.1b).

Other than the position solution, the velocity accuracy remains largely unaffected by the simulated error sources. In all cases, a 3D velocity error of 4-5 cm/s is obtained. At the given dilution of precision, this corresponds to an average range-rate noise of about 1.5 cm/s, which is slightly lower than suggested by the receiver noise analysis in Sect. 4.3. Except for a small along-track velocity bias of about -1.5 cm/s in Cases C & D, which can be attributed to the ionospheric path delays, no systematic velocity errors have been recognized.

For further illustration, the kinematic velocity errors in radial, along-track and normal direction are shown in Figs. 6.1b and 6.2.b for the errors-free scenario (Case A) and the scenario with ephemeris and ionospheric errors (Case D), respectively.

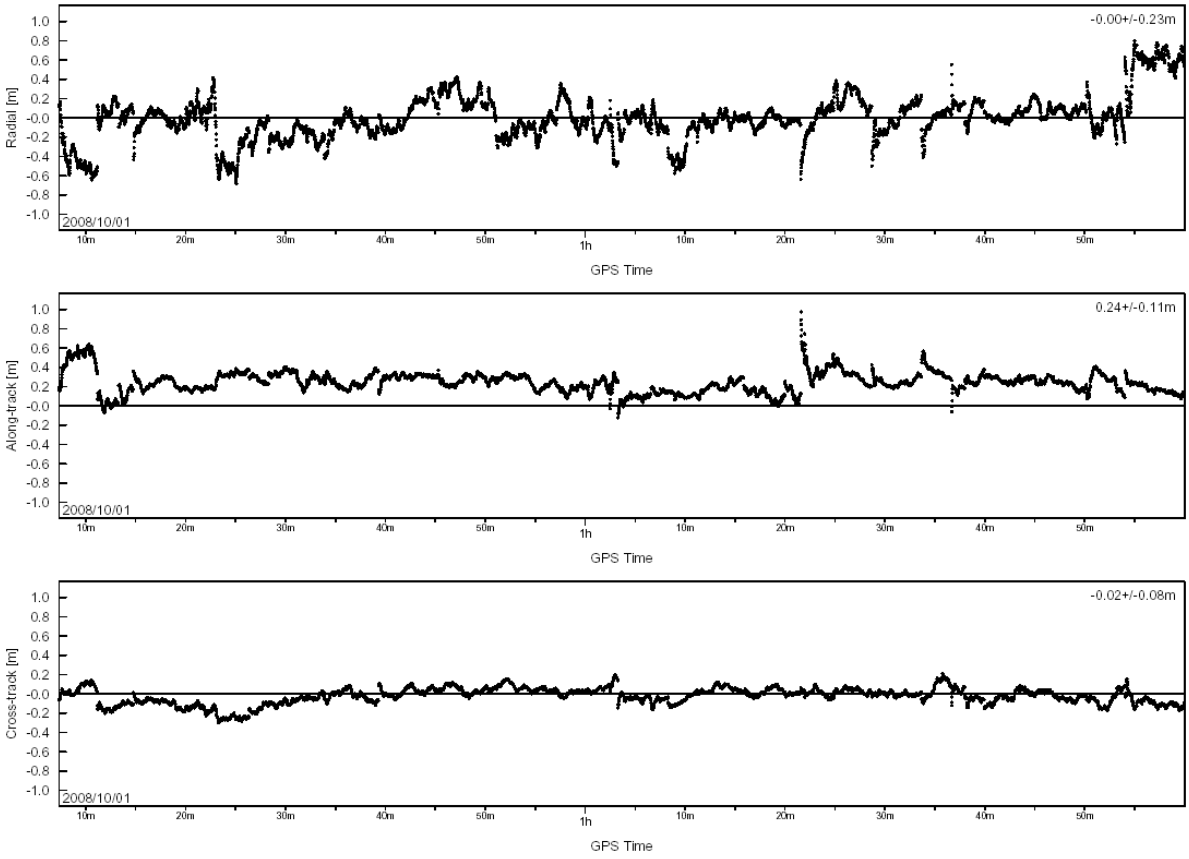

Fig. 6.1a Position errors in radial (*top*), along-track (*center*) and cross-track direction (*bottom*) of the kinematic Phoenix-S/XNS navigation solution over a 2h arc (error-free Aeolus scenario, Test Case A)

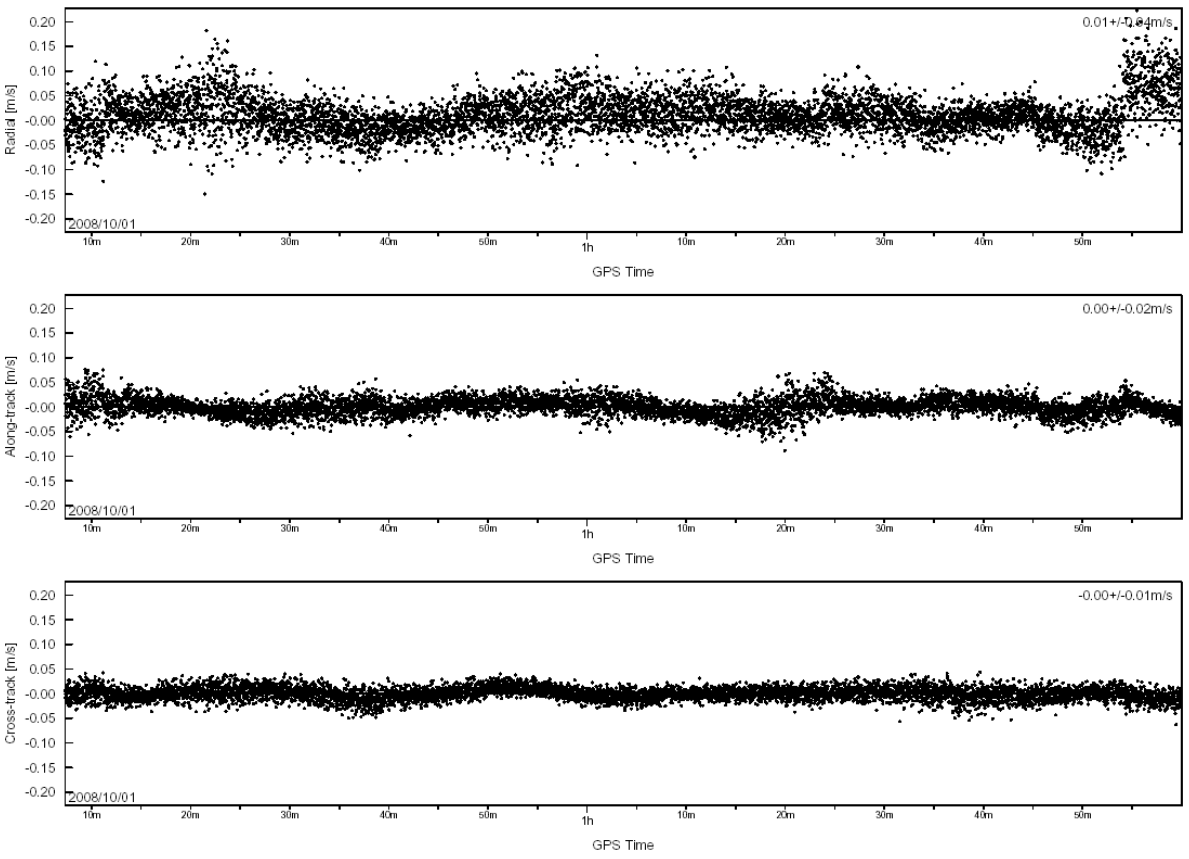

Fig. 6.1b Velocity errors in radial (*top*), along-track (*center*) and cross-track direction (*bottom*) of the kinematic Phoenix-S/XNS navigation solution over a 2h arc (error-free Aeolus scenario, Test Case A)

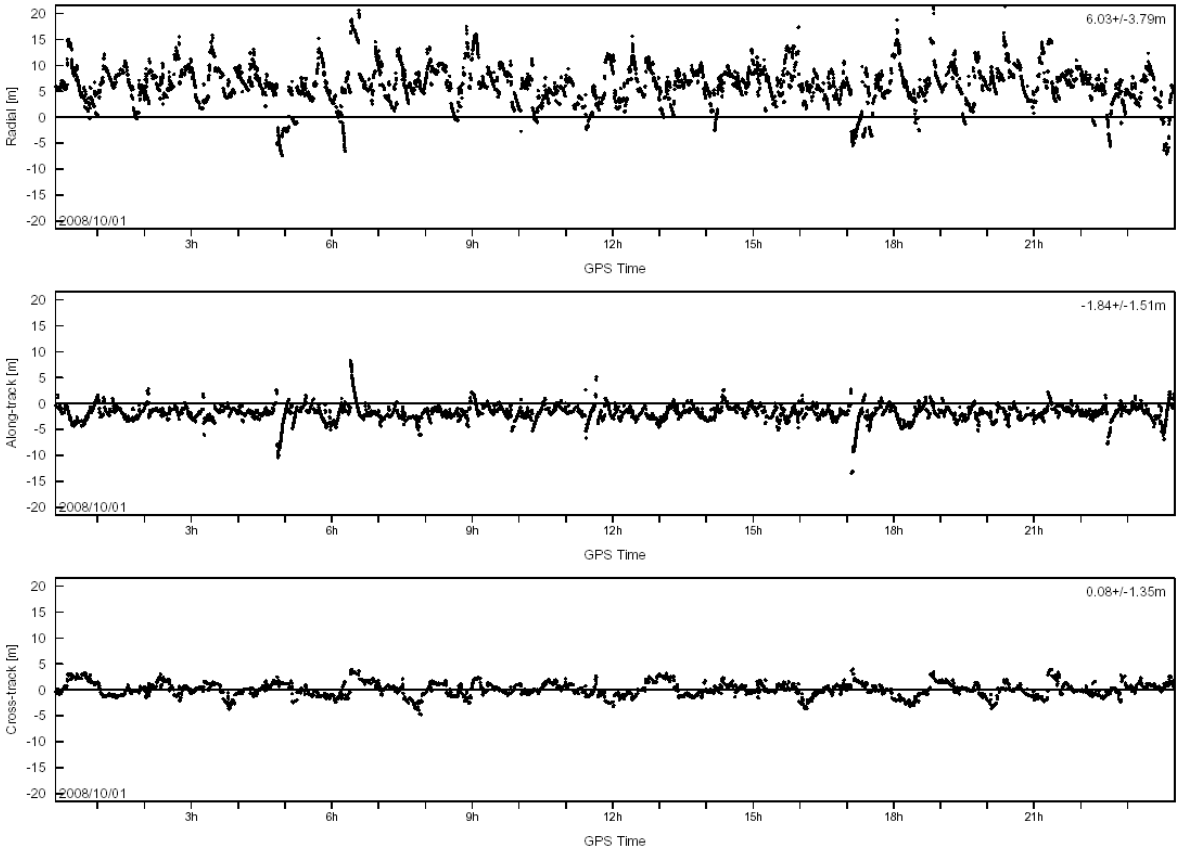

Fig. 6.2a Position errors in radial (*top*), along-track (*center*) and cross-track direction (*bottom*) of the kinematic Phoenix-S/XNS navigation solution over a 24h arc (Test Case D with ephemeris errors and ionospheric delays)

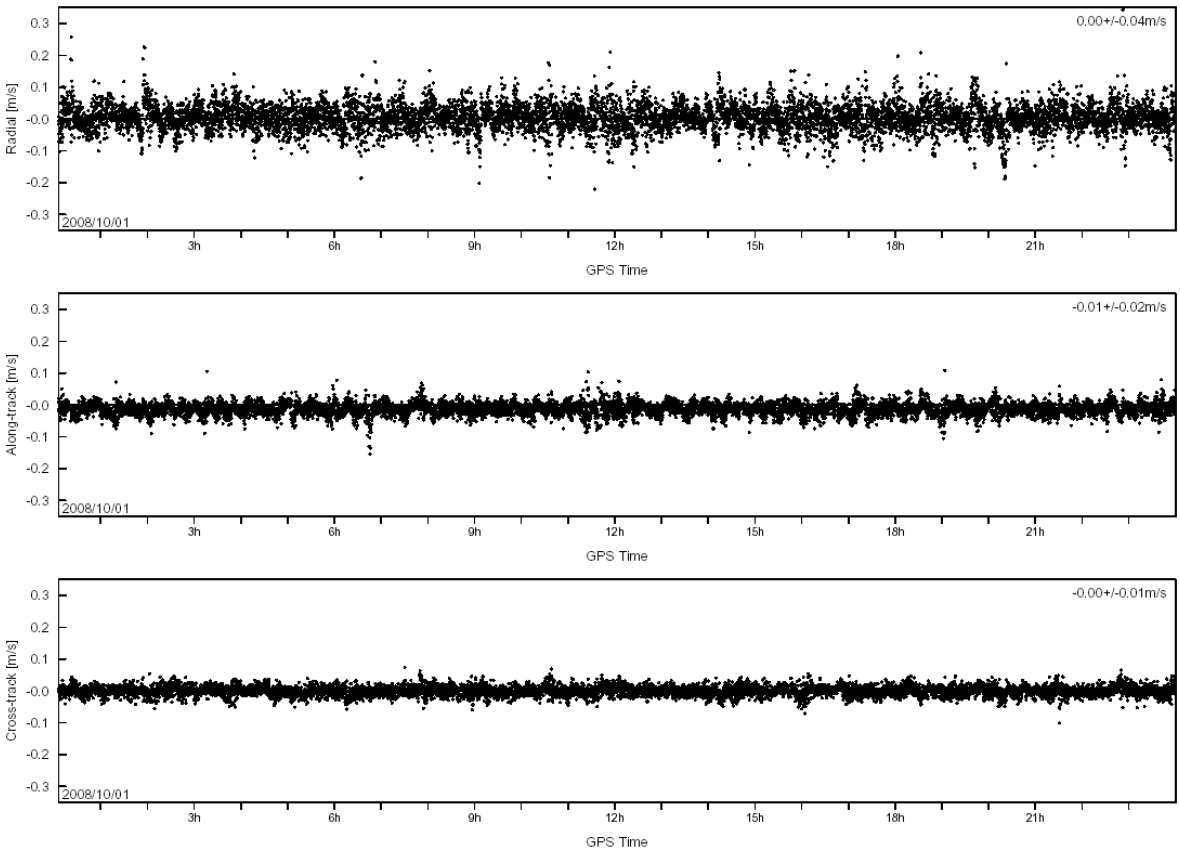

Fig. 6.2b Velocity errors in radial (*top*), along-track (*center*) and cross-track direction (*bottom*) of the kinematic Phoenix-S/XNS navigation solution over a 24h arc (Test Case D with ephemeris errors and ionospheric delays)

6.2 Dynamically Filtered Navigation Accuracy

In addition to a kinematic navigation solution, the Phoenix-XNS model can provide a dynamically filtered navigation solution within the F80 output message. As part of the Phoenix GPS receiver testing, the performance of the dynamically filtered navigation solution has been analyzed for different combinations of broadcast ephemeris errors and ionospheric errors (cf. Table 1.2.

The resulting position and velocity accuracies are collated in Table 6.2a/b. A graphical representation of the radial, along-track and cross-tack errors for the short data arcs is presented in Figs. 6.3a/b and 6.4a/b for an error-free scenario (Test Case A) and a scenario with ephemeris errors and ionospheric path delays (Test Case D).

Table 6.2a Dynamically filtered position solution accuracy of the Phoenix-XNS GPS receiver in the Aeolus test scenario

Case	Ephem. Errors	Iono. Errors	Arc	Radial [m]	Along-track [m]	Cross-track [m]	Position (3D rms)	Note
A	none	none	24h	-0.08 ± 0.58	+0.10 ± 0.40	+0.05 ± 0.26	0.77 m	#05, 070328
B	1.5m rms	none	24h	-0.05 ± 0.62	+0.09 ± 0.41	+0.06 ± 0.27	0.80 m	#05, 070402
C	none	10 TECU	24h	-0.03 ± 0.92	+0.05 ± 0.48	+0.05 ± 0.26	1.08 m	#05, 070328
D	1.5m rms	10 TECU	24h	-0.07 ± 0.74	+0.05 ± 0.48	+0.05 ± 0.27	0.93 m	#05, 070403

Table 6.2b Dynamically filtered velocity solution accuracy of the Phoenix-XNS GPS receiver in the Aeolus test scenario

Case	Ephem. Errors	Iono. Errors	Arc	Radial [m/s]	Along-track [m/s]	Cross-track [m/s]	Velocity (3D rms)	Note
A	none	none	24h	-0.000±0.001	+0.000±0.001	+0.000±0.001	0.002 m/s	#05, 070328
B	1.5m rms	none	23h	-0.000±0.002	+0.000±0.001	+0.000±0.001	0.002 m/s	#05, 070402
C	none	10 TECU	24h	-0.000±0.001	+0.000±0.001	+0.000±0.001	0.001 m/s	#05, 070329
D	1.5m rms	10 TECU	24h	-0.000±0.002	+0.000±0.001	+0.000±0.001	0.002 m/s	#05, 070403

The filtered position solution is typically accurate to 1.0 m in all test cases. In the absence of broadcast ephemeris errors and ionospheric path delays (Case A) its accuracy is roughly comparable to that of the kinematic position solution. This may be understood by the fact that both the carrier phase smoothing and the dynamical filtering provide a high level of noise reduction and thus enable a very accurate position solution. However, the dynamical filtering improves the accuracy of the velocity solution by almost two orders of magnitude compared to its kinematic counterpart.

A major benefit of the dynamical filtering is also evident in the presence of ionospheric path delays (Case C). These are fully compensated in the Phoenix-XNS navigation system through the use of ionosphere-free GRAPHIC measurements. In addition, the dynamical filtering can partly reduce the impact of broadcast ephemeris errors on the navigation solution (Case B). Overall, the XNS is thus able to provide a one meter navigation accuracy and a one mm/s velocity accuracy under representative conditions of ephemeris errors and ionospheric delays (Case D).

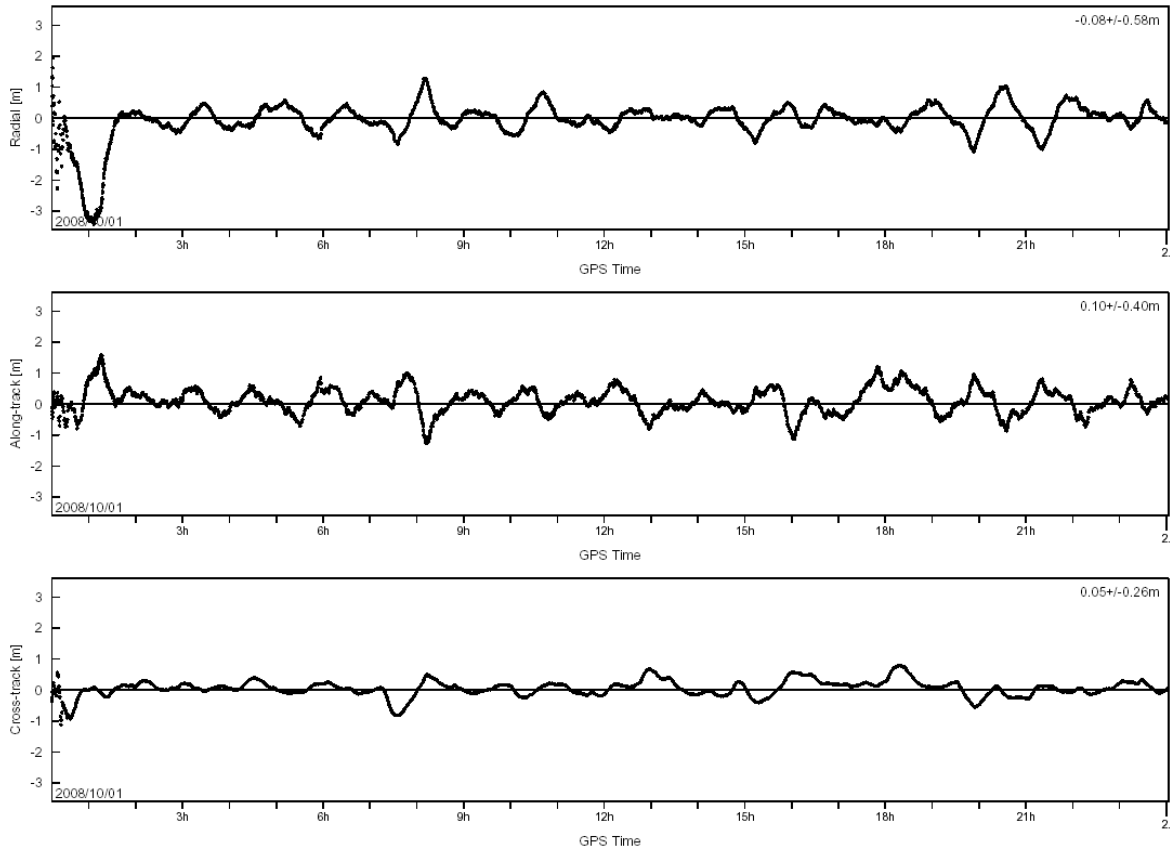

Fig. 6.3a Position errors in radial (*top*), along-track (*center*) and cross-track direction (*bottom*) of the dynamic Phoenix GPS navigation solution over a 24h arc (error-free Aeolus scenario, test case A)

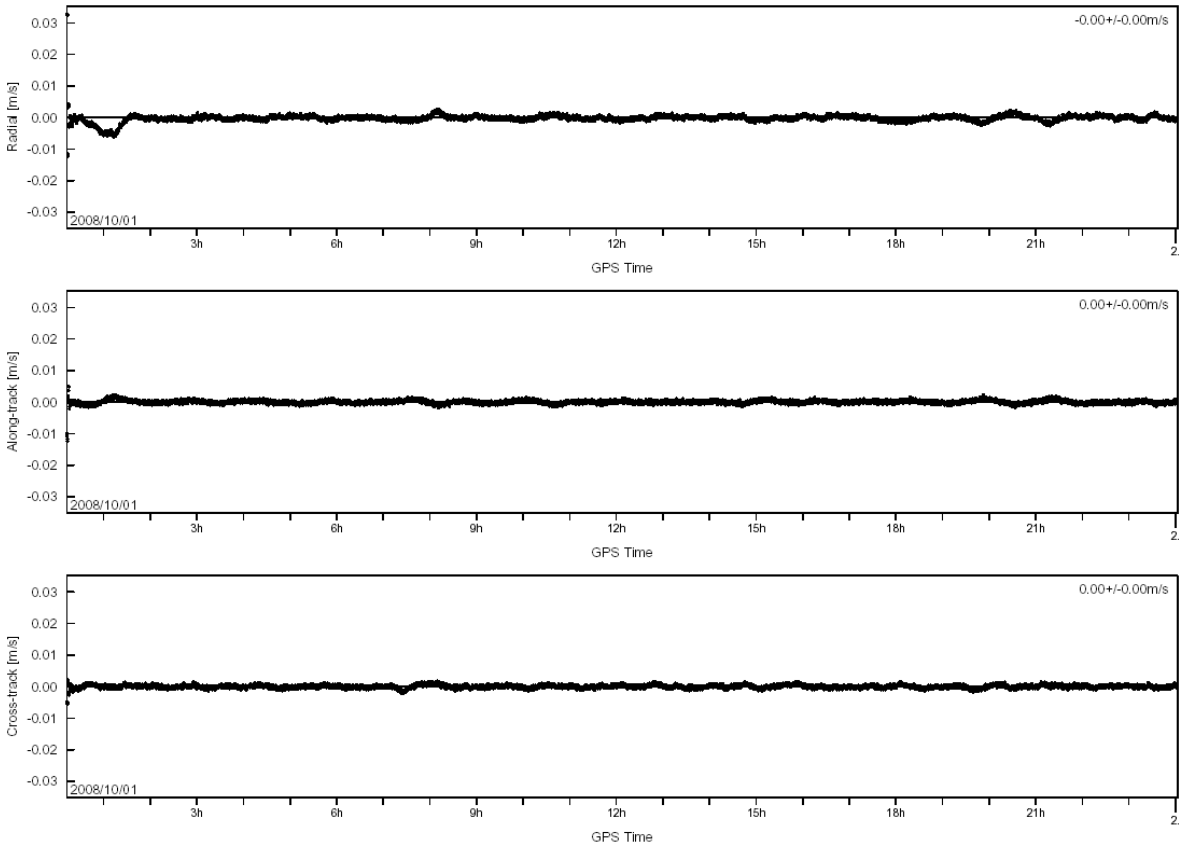

Fig. 6.3b Velocity errors in radial (*top*), along-track (*center*) and cross-track direction (*bottom*) of the dynamic Phoenix GPS navigation solution over a 24h arc (error-free Aeolus scenario, test case A)

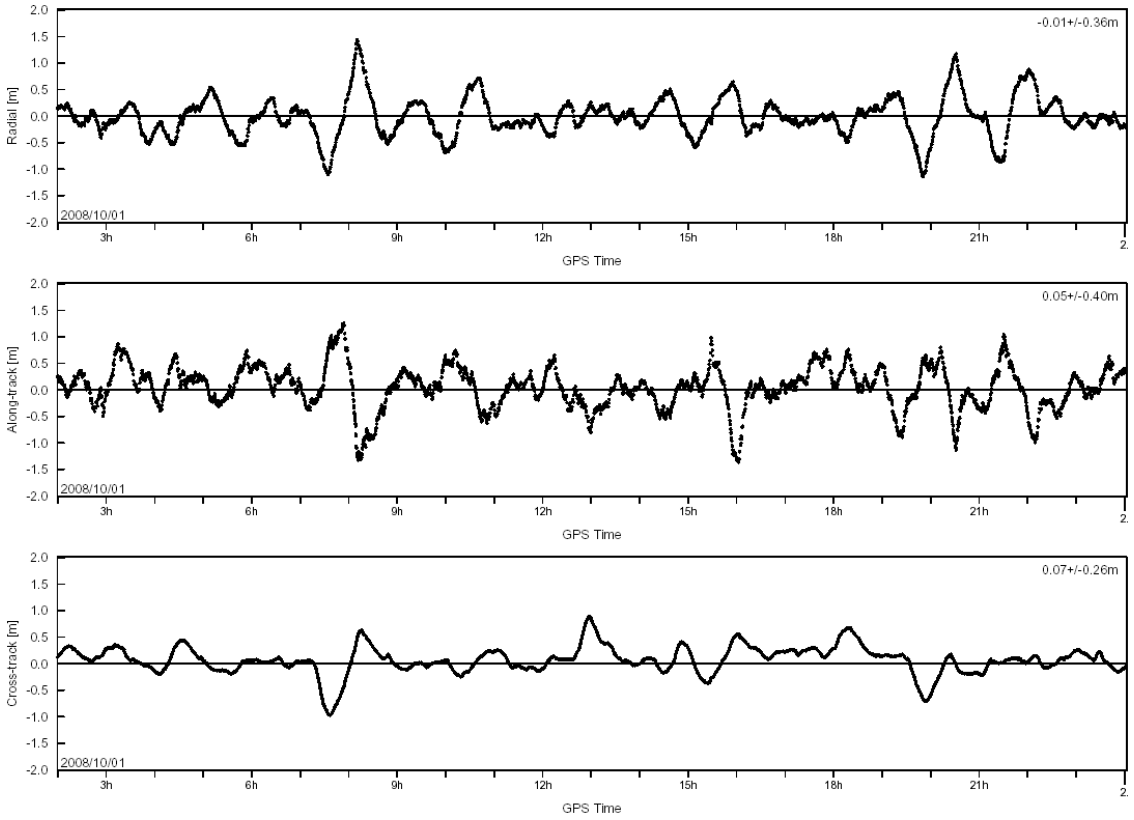

Fig. 6.4a Position errors in radial (*top*), along-track (*center*) and cross-track direction (*bottom*) of the dynamic Phoenix GPS navigation solution over a 22h arc (steady-state phase of Test Case D with ephemeris errors and ionospheric delays)

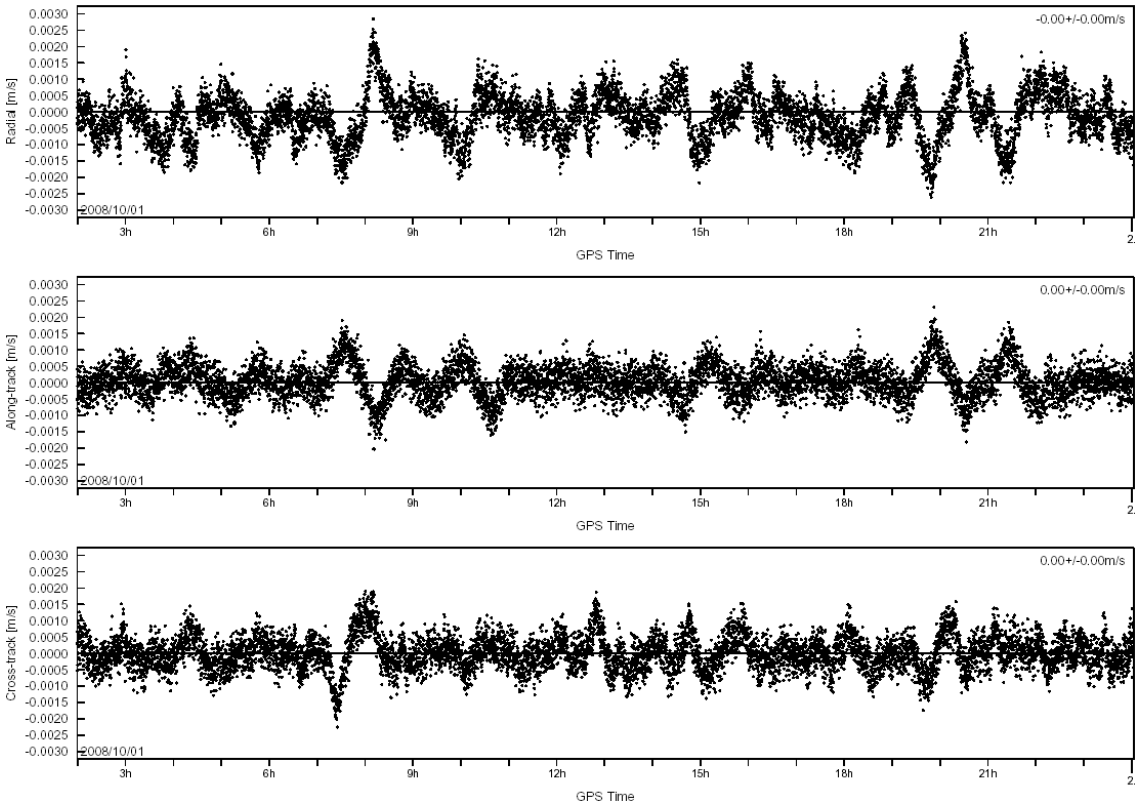

Fig. 6.4b Velocity errors in radial (*top*), along-track (*center*) and cross-track direction (*bottom*) of the dynamic Phoenix GPS navigation solution over a 22h arc (steady state phase of Test Case D with ephemeris errors and ionospheric delays)

During the initial acquisition of the Kalman-filter, errors comparable to the kinematic navigation solution may be observed. This acquisition phase takes between 30 min and 2 hours and is illustrated in Fig. 6.5 for test case D. Evidently, the accuracy during the start-up phase suffers from the degraded initial state vector, which exhibits a pronounced radial bias due to ionospheric path delays. At this stage, discontinuities of the position (and velocity) solution may, furthermore, be noted that reflect the measurement update interval of 30s. In between two updates, the solution is determined from an interpolating polynomial, which ensures a local smoothness.

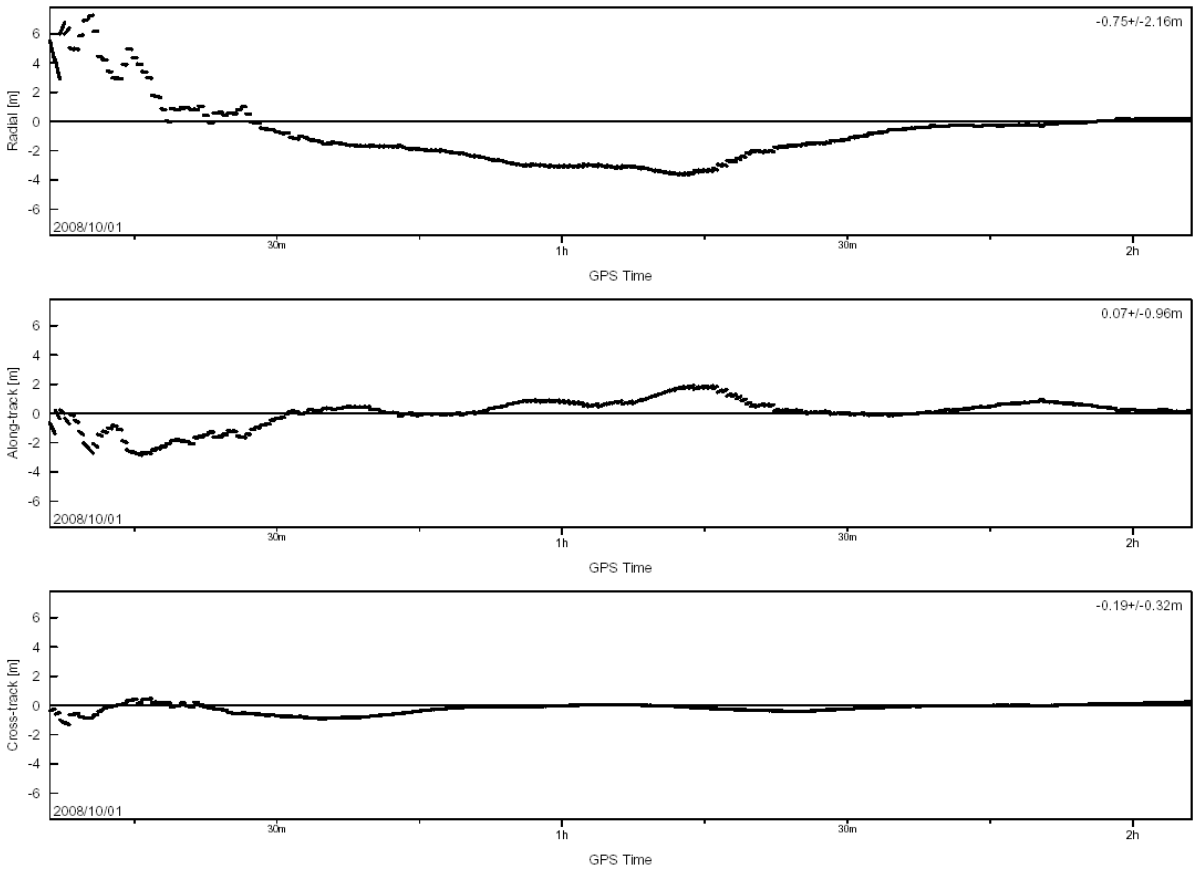

Fig. 6.5 Position errors in radial (*top*), along-track (*center*) and cross-track direction (*bottom*) of the dynamic Phoenix GPS navigation solution after filter initialization (Test Case D with ephemeris errors and ionospheric delays)

6.3 POD Performance

For an in-flight performance verification of the Phoenix GPS navigation accuracy, a precise reference orbit will be required in future mission. Even if the host spacecraft does not offer an independent source of navigation information (such as a dual-frequency receiver or laser retro-reflector), it is still possible to generate orbit information of adequate accuracy by post-processing of the raw GPS measurements delivered by the Phoenix receiver itself.

Compared to the real-time navigation solution, a much higher accuracy can be achieved in post-processing due to the availability of precise GPS orbit and clock data and the use of advanced orbit determination algorithms. To overcome the limitation of ionospheric path delays in the processing of single-frequency raw measurements, the ionosphere-free GRAPHIC combination (=½ (C1+LA)) is formed from C/A code and L1 phase measurements (see e.g. [19]). In this way ionospheric effects can be rigorously eliminated and the resulting data noise is half that of the pseudorange noise (i.e. 0.25 m instead of 0.5 m for the Phoenix GPS receiver, cf. Fig. 6.6). Using this approach, a reduced dynamic orbit adjustment can provide a reconstructed Aeolus orbit with a 3D position accuracy of about 0.2 m. This information can then be used in the science data processing or to assess the real-time navigation solution provided by the Phoenix GPS receiver.

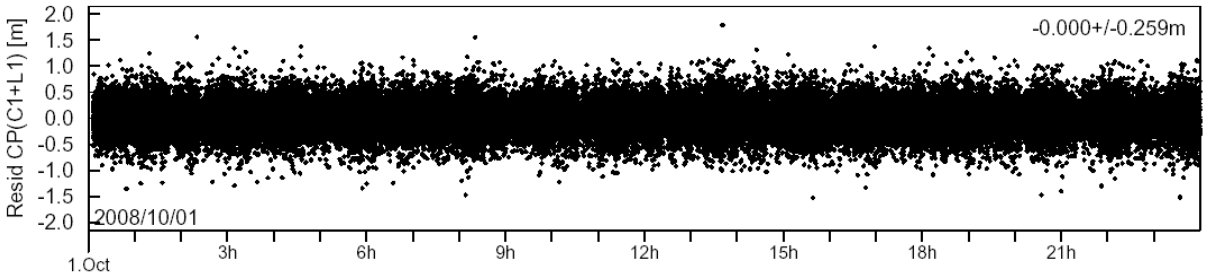

Fig. 6.6 GRAPHIC residuals from reduced dynamic orbit determination for Aeolus Test Case D.

The suitability of this approach has been verified with measurements from an 24 h test run (Dase D) that were processed in DLR's GHOST software [20]. Since precise IGS ephemeris products for the GPS satellites provide accuracies in the sub-decimeter range, ephemeris error have been neglected in this analysis. The achieved position results are summarized in Table 6.3 and Fig. 6.7. The associated velocities are typically accurate to better than 1 mm/s.

Table 6.3 Precise orbit determination results (residuals and position error) obtained in the post-processing of Phoenix GRAPHIC data for a 24h data arc (Aeolus Test Case D with precise GPS ephemerides).

Data	Residuals	Radial	Along-track	Cross-track	Position (3D rms)
GRAPHIC (C1+LA)	0.25 m	-0.03 ± 0.04 m	+0.15 ± 0.07 m	+0.09 ± 0.03 m	0.20 m

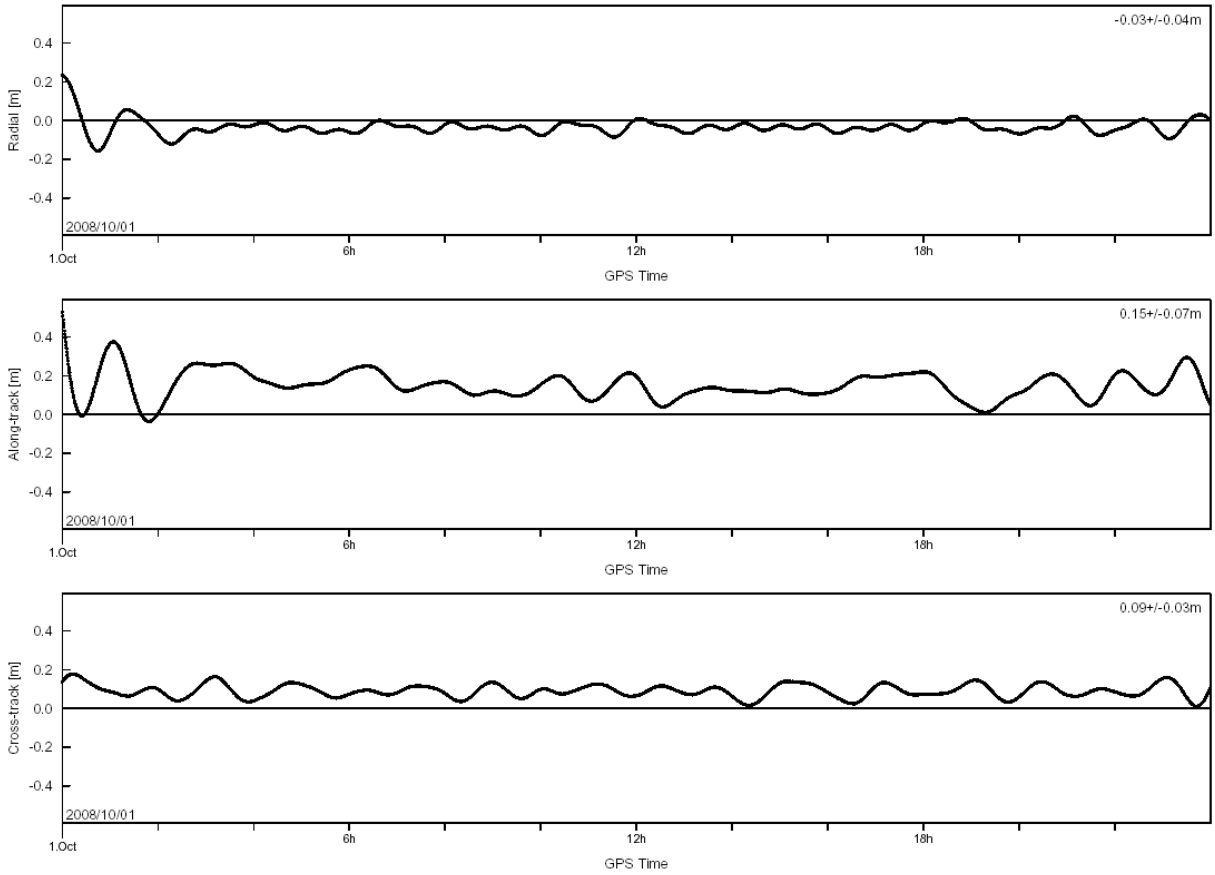

Fig. 6.7 Reduced dynamic orbit determination errors based on Phoenix GRAPHIC measurements collected in a 24h data arc (Aeolus Test Case D with precise GPS ephemerides).

Summary and Conclusions

Extensive signal simulator tests have been conducted to validate the tracking and navigation performance of the Phoenix GPS receiver for satellites in low Earth orbit.

The results confirm a high quality of the Phoenix raw measurements. Representative noise values of 0.5 m, 0.8 mm and 0.1 m/s are obtained for pseudorange, carrier phase and Doppler date, respectively, at average C/N_0 values of 42 dB-Hz. For use within the kinematic navigation solution, smoothed pseudoranges with a noise level of about 0.1 m and range-rate measurements from time-differenced carrier phases with a noise level of 2 cm/s are, furthermore, available.

All measurements are synchronized to integer seconds of GPS times and a pulse-per-second signal is issued with a maximum offset of 200ns from the nominal value. Double-difference carrier phases exhibit integer ambiguities for use in differential positioning techniques.

After a cold start, a first navigation fix is typically obtained within nine minutes and the TTF did not exceed 15 min in 92% of all test cases. The hot start time, in contrast is typically less than 30s.

The accuracy of the kinematic navigation solution is generally better than 10 m and 5 cm/s (3D rms) for typical values of the ionospheric path delays and broadcast ephemeris errors. In the absence of such errors, a position accuracy of better than 1m is achieved. A systematic along-track bias of typically 0.5 m can be noted in the kinematic navigation solution, which varies between different receiver units and is best attributed to the characteristics of the front-tend hardware.

Supplementary to the kinematic navigation solution, a dynamically filtered state vector is available in the Phoenix-XNS model. Here, accuracies of roughly 1 m and 2 mm/s have been demonstrated under various conditions of ionospheric path delays and broadcast ephemeris errors.

References

[1] *Phoenix Spaceborne GPS Receiver*; Datasheet; DLR/GSOC, Issue 1.0, 1 Dec. 2005.

[2] Montenbruck O., Markgraf M.; *User's Manual for the Phoenix GPS Receiver*; DLR/GSOC; GTN-MAN-120, Issue 1.7, 6 June 2006.

[3] Montenbruck O., Gill E.; *User's Manual for the Phoenix-XNS Navigation System*; DLR/GSOC; GTN-MAN-0130; Deutsches Zentrum für Luft- und Raumfahrt, Oberpfaffenhofen, Issue 1.0 (2006).

[4] Montenbruck O., Gill E., Markgraf M.; *Phoenix-XNS - A Miniature Real-Time Navigation System for LEO Satellites*; 3rd ESA Workshop on Satellite Navigation User Equipment Technologies, NAVITEC'2006, 11-13 December 2006, Noordwijk (2006).

[5] *STR4500 GPS/SBAS Simulator with SimPLEX Software User Manual*; DGP00603AAA; Issue 1.11, Jan 2005.

[6] Montenbruck O., Garcia-Fernandez M.; *Performance Testing of the MosaicGNSS Receiver for ADM-Aeolus*; AEO-DLR-TST-010; Deutsches Zentrum für Luft- und Raumfahrt, Oberpfaffenhofen (2005).

[7] *SimGEN (Including SimLocate) User Manual – Software for the Spirent Range of Satellite Navigation Simulator Products*; DGP00686AAA; Issue 1-05, Aug. 2003.

[8] Standardization Agreement on NAVSTAR Global Positioning System (GPS) System Characteristics; STANAG 4294; North Atlantic Treaty Organization (NATO), Military Agency for Standardization (MAS); Edition 1, 13 May 1993.

[9] Van Dierendonck A. J.; *GPS Receivers*; chap. 8 in: Spilker J., Parkinson B., eds.; *Global Positioning System: Theory and Applications Vol. I*; American Institute of Aeronautics and Astronautics Inc., Washington (1995).

[10] Montenbruck O., Holt G.; *Spaceborne GPS Receiver Performance Testing*; DLR-GSOC TN 02-04; Deutsches Zentrum für Luft- und Raumfahrt, Oberpfaffenhofen (2002).

[11] Lear W.M.; *GPS Navigation for Low-Earth Orbiting Vehicles*; NASA 87-FM-2, Rev. 1; JSC-32031, Lyndon B. Johnson Space Center; Houston, Texas (1987).

[12] Renaudie C.; *Acquisition Test for the Phoenix GPS Receiver*; DLR-GSOC TN 06-02; Deutsches Zentrum für Luft- und Raumfahrt, Oberpfaffenhofen (2006).

[13] Montenbruck O., Garcia-Fernandez M., Williams J.; *Performance Comparison of Semi-Codeless GPS Receivers for LEO Satellites*; GPS Solutions **10**,249-261(2006). DOI 10.1007/s10291-006-0025-9

[14] Ward P.; *Satellite Signal Acquisition and Tracking*; chap. 5 in: Kaplan E. D. ed.; *Understanding GPS Principles and Applications*; Artech House Publishers (1996).

[15] Montenbruck O., Ebinuma T., Lightsey E.G., Leung S.; *A Real-Time Kinematic GPS Sensor for Spacecraft Relative Navigation*; Aerospace Science and Technology 6, 435-449 (2002).

[16] Gurtner W., Estey L.; *RINEX Version 2.20 -Modifications to Accommodate Low Earth Orbiter Data*; April 15, 2002. URL ftp://ftp.aiub.unibe.ch/aiub/rinex/rnx_leo.txt ;last accessed 29 Sep 2005.

[17] Montenbruck O.; *Code Tracking Loop Enhancement for the Mitel Architect/Orion Receiver*; DLR-GSOC TN 03-03; Deutsches Zentrum für Luft- und Raumfahrt, Oberpfaffenhofen (2003).

[18] Garcia-Fernandez M., Montenbruck O.; *LEO Satellite Navigation Errors and VTEC in Single-Frequency GPS Tracking*; Radio Science **41**, RS5001 (2006). DOI 10.1029/2005RS003420.

[19] W. Bertiger, S.-C Wu, *Single frequency GPS orbit determination for low earth orbiters*, in: National Technical Meeting, Institute of Navigation, January 1996, Santa Monica, CA, 1996.

[20] Montenbruck O., van Helleputte T., Kroes R., Gill E.; *Reduced Dynamic Orbit Determination using GPS Code and Carrier Measurements*; Aerospace Science and Technology **9/3**, 261-271 (2005).

Annex

A.1 YUMA Almanac for DLR_AEO Scenario

The following listing provides the YUMA almanac for week 1333 (=1024+309).

```
******** Week  309 almanac for PRN-01 ********
ID:                         01
Health:                     063
Eccentricity:               0.5852222443E-002
Time of Applicability(s):  589824.0000
Orbital Inclination(rad):   0.9844465517
Rate of Right Ascen(r/s):  -0.7748894201E-008
SQRT(A)  (m 1/2):           5153.608398
Right Ascen at Week(rad):   0.1661531515E+001
Argument of Perigee(rad):  -1.703451210
Mean Anom(rad):            -0.2275620801E+001
Af0(s):                     0.9536743164E-006
Af1(s/s):                   0.3637978807E-011
week:                       1333

******** Week  309 almanac for PRN-02 ********
ID:                         02
Health:                     000
Eccentricity:               0.9191989899E-002
Time of Applicability(s):  589824.0000
Orbital Inclination(rad):   0.9540965021
Rate of Right Ascen(r/s):  -0.7817468486E-008
SQRT(A)  (m 1/2):           5153.539062
Right Ascen at Week(rad):  -0.4653732941E+000
Argument of Perigee(rad):   1.892715453
Mean Anom(rad):            -0.8191929286E+000
Af0(s):                    -0.2670288086E-004
Af1(s/s):                   0.0000000000E+000
week:                       1333

******** Week  309 almanac for PRN-03 ********
ID:                         03
Health:                     000
Eccentricity:               0.6988525391E-002
Time of Applicability(s):  589824.0000
Orbital Inclination(rad):   0.9264009584
Rate of Right Ascen(r/s):  -0.8137481816E-008
SQRT(A)  (m 1/2):           5153.570801
Right Ascen at Week(rad):  -0.1598005760E+001
Argument of Perigee(rad):   0.594643383
Mean Anom(rad):            -0.1668291367E+001
Af0(s):                     0.2193450928E-004
Af1(s/s):                   0.3637978807E-011
week:                       1333

******** Week  309 almanac for PRN-04 ********
ID:                         04
Health:                     000
Eccentricity:               0.6991863251E-002
Time of Applicability(s):  589824.0000
Orbital Inclination(rad):   0.9537369754
Rate of Right Ascen(r/s):  -0.7840326581E-008
SQRT(A)  (m 1/2):           5153.622070
Right Ascen at Week(rad):  -0.4454607554E+000
Argument of Perigee(rad):   0.049545782
Mean Anom(rad):             0.1659683697E+001
Af0(s):                     0.5531311035E-004
Af1(s/s):                  -0.2546585165E-010
week:                       1333

******** Week  309 almanac for PRN-05 ********
ID:                         05
Health:                     000
Eccentricity:               0.6355762482E-002
Time of Applicability(s):  589824.0000
Orbital Inclination(rad):   0.9371268397
Rate of Right Ascen(r/s):  -0.8046049436E-008
SQRT(A)  (m 1/2):           5153.707520
Right Ascen at Week(rad):  -0.2638709485E+001
Argument of Perigee(rad):   0.965913922
Mean Anom(rad):             0.1337710643E+001
Af0(s):                     0.1182556152E-003
Af1(s/s):                   0.3637978807E-011
week:                       1333

******** Week  309 almanac for PRN-06 ********
ID:                         06
Health:                     000
Eccentricity:               0.6385803223E-002
Time of Applicability(s):  589824.0000
Orbital Inclination(rad):   0.9338970910
Rate of Right Ascen(r/s):  -0.8034620388E-008
SQRT(A)  (m 1/2):           5153.685547
Right Ascen at Week(rad):  -0.1541712485E+001
Argument of Perigee(rad):  -1.897181074
Mean Anom(rad):             0.2537761864E+001
Af0(s):                     0.7486343384E-003
Af1(s/s):                   0.2546585165E-010
week:                       1333

******** Week  309 almanac for PRN-07 ********
ID:                         07
Health:                     000
Eccentricity:               0.1343441010E-001
Time of Applicability(s):  589824.0000
Orbital Inclination(rad):   0.9354730166
Rate of Right Ascen(r/s):  -0.7988904198E-008
SQRT(A)  (m 1/2):           5153.687012
Right Ascen at Week(rad):  -0.1568748897E+001
Argument of Perigee(rad):  -1.785687336
Mean Anom(rad):            -0.1563824504E+001
Af0(s):                     0.2565383911E-003
Af1(s/s):                   0.2182787284E-010
week:                       1333

******** Week  309 almanac for PRN-08 ********
ID:                         08
Health:                     000
Eccentricity:               0.9391307831E-002
Time of Applicability(s):  589824.0000
Orbital Inclination(rad):   0.9696040892
Rate of Right Ascen(r/s):  -0.7611745631E-008
SQRT(A)  (m 1/2):           5153.664551
Right Ascen at Week(rad):   0.2714027342E+001
Argument of Perigee(rad):   2.554465252
Mean Anom(rad):             0.2636792009E+001
Af0(s):                    -0.3719329834E-004
Af1(s/s):                   0.0000000000E+000
week:                       1333

******** Week  309 almanac for PRN-09 ********
ID:                         09
Health:                     000
Eccentricity:               0.1715946198E-001
Time of Applicability(s):  589824.0000
Orbital Inclination(rad):   0.9568768423
Rate of Right Ascen(r/s):  -0.7726036106E-008
SQRT(A)  (m 1/2):           5153.612793
Right Ascen at Week(rad):   0.2638935312E+001
Argument of Perigee(rad):   1.167446265
Mean Anom(rad):             0.2232159635E+001
Af0(s):                    -0.9536743164E-006
Af1(s/s):                  -0.3637978807E-011
week:                       1333

******** Week  309 almanac for PRN-10 ********
ID:                         10
Health:                     000
Eccentricity:               0.6492137909E-002
Time of Applicability(s):  589824.0000
Orbital Inclination(rad):   0.9773219300
Rate of Right Ascen(r/s):  -0.7931758961E-008
SQRT(A)  (m 1/2):           5153.657227
Right Ascen at Week(rad):   0.5996763830E+000
Argument of Perigee(rad):   0.368235159
Mean Anom(rad):            -0.4302123272E+000
Af0(s):                     0.6771087646E-004
Af1(s/s):                   0.0000000000E+000
week:                       1333
```

```
******** Week  309 almanac for PRN-11 ********
ID:                         11
Health:                     000
Eccentricity:               0.4296779633E-002
Time of Applicability(s):  589824.0000
Orbital Inclination(rad):   0.9009165041
Rate of Right Ascen(r/s):  -0.8286059433E-008
SQRT(A)  (m 1/2):           5153.609863
Right Ascen at Week(rad):  -0.5944227984E+000
Argument of Perigee(rad):   0.234284107
Mean Anom(rad):            -0.3091516944E+001
Af0(s):                     0.2508163452E-003
Af1(s/s):                   0.3637978807E-011
week:                       1333

******** Week  309 almanac for PRN-13 ********
ID:                         13
Health:                     000
Eccentricity:               0.2731323242E-002
Time of Applicability(s):  589824.0000
Orbital Inclination(rad):   0.9886410304
Rate of Right Ascen(r/s):  -0.7703178011E-008
SQRT(A)  (m 1/2):           5153.646973
Right Ascen at Week(rad):   0.1646012693E+001
Argument of Perigee(rad):   1.084094108
Mean Anom(rad):            -0.5639338067E+000
Af0(s):                     0.7629394531E-005
Af1(s/s):                   0.0000000000E+000
week:                       1333

******** Week  309 almanac for PRN-14 ********
ID:                         14
Health:                     000
Eccentricity:               0.1740932465E-002
Time of Applicability(s):  589824.0000
Orbital Inclination(rad):   0.9829305472
Rate of Right Ascen(r/s):  -0.7771752296E-008
SQRT(A)  (m 1/2):           5153.702148
Right Ascen at Week(rad):   0.1634478251E+001
Argument of Perigee(rad):  -2.001023260
Mean Anom(rad):            -0.1406666749E+001
Af0(s):                    -0.2765655518E-004
Af1(s/s):                   0.0000000000E+000
week:                       1333

******** Week  309 almanac for PRN-15 ********
ID:                         15
Health:                     000
Eccentricity:               0.9157180786E-002
Time of Applicability(s):  589824.0000
Orbital Inclination(rad):   0.9608496129
Rate of Right Ascen(r/s):  -0.7771752296E-008
SQRT(A)  (m 1/2):           5153.478027
Right Ascen at Week(rad):  -0.3901359556E+000
Argument of Perigee(rad):   2.469097124
Mean Anom(rad):             0.2594396315E+001
Af0(s):                     0.4673004150E-003
Af1(s/s):                   0.7275957614E-011
week:                       1333

******** Week  309 almanac for PRN-16 ********
ID:                         16
Health:                     000
Eccentricity:               0.2942562103E-002
Time of Applicability(s):  589824.0000
Orbital Inclination(rad):   0.9617903745
Rate of Right Ascen(r/s):  -0.7771752296E-008
SQRT(A)  (m 1/2):           5153.746094
Right Ascen at Week(rad):  -0.2555440094E+001
Argument of Perigee(rad):  -1.053845550
Mean Anom(rad):             0.1149150099E+001
Af0(s):                     0.5722045898E-005
Af1(s/s):                   0.0000000000E+000
week:                       1333

******** Week  309 almanac for PRN-18 ********
ID:                         18
Health:                     000
Eccentricity:               0.6338596344E-002
Time of Applicability(s):  589824.0000
Orbital Inclination(rad):   0.9612391002
Rate of Right Ascen(r/s):  -0.8080336578E-008
SQRT(A)  (m 1/2):           5153.564453
Right Ascen at Week(rad):   0.6259019867E+000
Argument of Perigee(rad):  -2.789249326
Mean Anom(rad):             0.1070463551E+001
Af0(s):                    -0.1754760742E-003
Af1(s/s):                  -0.3637978807E-011
week:                       1333

******** Week  309 almanac for PRN-19 ********
ID:                         19
Health:                     000
Eccentricity:               0.3421783447E-002
Time of Applicability(s):  589824.0000
Orbital Inclination(rad):   0.9584887206
Rate of Right Ascen(r/s):  -0.7783181344E-008
SQRT(A)  (m 1/2):           5153.658691
Right Ascen at Week(rad):  -0.1455960488E+001
Argument of Perigee(rad):  -1.580177728
Mean Anom(rad):            -0.1372980216E-001
Af0(s):                    -0.2479553223E-004
Af1(s/s):                   0.0000000000E+000
week:                       1333

******** Week  309 almanac for PRN-20 ********
ID:                         20
Health:                     000
Eccentricity:               0.2594470978E-002
Time of Applicability(s):  589824.0000
Orbital Inclination(rad):   0.9609694551
Rate of Right Ascen(r/s):  -0.8080336578E-008
SQRT(A)  (m 1/2):           5153.616699
Right Ascen at Week(rad):   0.5732837492E+000
Argument of Perigee(rad):   1.484943961
Mean Anom(rad):             0.6356485321E+000
Af0(s):                    -0.5435943604E-004
Af1(s/s):                   0.0000000000E+000
week:                       1333

******** Week  309 almanac for PRN-21 ********
ID:                         21
Health:                     000
Eccentricity:               0.1028013229E-001
Time of Applicability(s):  589824.0000
Orbital Inclination(rad):   0.9473433914
Rate of Right Ascen(r/s):  -0.7874613724E-008
SQRT(A)  (m 1/2):           5153.569824
Right Ascen at Week(rad):  -0.4233648407E+000
Argument of Perigee(rad):  -3.079560433
Mean Anom(rad):             0.2447566715E+001
Af0(s):                     0.1173019409E-003
Af1(s/s):                   0.3637978807E-011
week:                       1333

******** Week  309 almanac for PRN-22 ********
ID:                         22
Health:                     000
Eccentricity:               0.4766941071E-002
Time of Applicability(s):  589824.0000
Orbital Inclination(rad):   0.9586984445
Rate of Right Ascen(r/s):  -0.8103194673E-008
SQRT(A)  (m 1/2):           5153.630371
Right Ascen at Week(rad):   0.6347066469E+000
Argument of Perigee(rad):  -1.570429310
Mean Anom(rad):            -0.6823600447E+000
Af0(s):                     0.3242492676E-004
Af1(s/s):                   0.0000000000E+000
week:                       1333

******** Week  309 almanac for PRN-23 ********
ID:                         23
Health:                     000
Eccentricity:               0.4230499268E-002
Time of Applicability(s):  589824.0000
Orbital Inclination(rad):   0.9651339733
Rate of Right Ascen(r/s):  -0.7943188009E-008
SQRT(A)  (m 1/2):           5153.610840
Right Ascen at Week(rad):   0.1626140975E+001
Argument of Perigee(rad):   2.287457096
Mean Anom(rad):            -0.1245595396E+001
Af0(s):                     0.1831054687E-003
Af1(s/s):                  -0.3637978807E-011
week:                       1333

******** Week  309 almanac for PRN-24 ********
ID:                         24
Health:                     000
Eccentricity:               0.8864402771E-002
Time of Applicability(s):  589824.0000
Orbital Inclination(rad):   0.9640374167
Rate of Right Ascen(r/s):  -0.7726036106E-008
SQRT(A)  (m 1/2):           5153.630859
Right Ascen at Week(rad):  -0.4146399505E+000
Argument of Perigee(rad):  -1.127400978
Mean Anom(rad):            -0.2809770813E+001
```

```
Af0(s):                       0.3528594971E-004
Af1(s/s):                     0.3637978807E-011
week:                         1333

******** Week  309 almanac for PRN-25 ********
ID:                           25
Health:                       000
Eccentricity:                 0.1197957993E-001
Time of Applicability(s):  589824.0000
Orbital Inclination(rad):     0.9501057552
Rate of Right Ascen(r/s):  -0.7817468486E-008
SQRT(A)  (m 1/2):             5153.697754
Right Ascen at Week(rad):     0.2586313330E+001
Argument of Perigee(rad):  -1.445005034
Mean Anom(rad):               0.3011403899E+001
Af0(s):                       0.9918212891E-004
Af1(s/s):                     0.0000000000E+000
week:                         1333

******** Week  309 almanac for PRN-26 ********
ID:                           26
Health:                       000
Eccentricity:                 0.1655626297E-001
Time of Applicability(s):  589824.0000
Orbital Inclination(rad):     0.9868733572
Rate of Right Ascen(r/s):  -0.7726036106E-008
SQRT(A)  (m 1/2):             5153.560059
Right Ascen at Week(rad):     0.1647596483E+001
Argument of Perigee(rad):     0.722572362
Mean Anom(rad):              -0.2220807952E+001
Af0(s):                       0.1907348633E-004
Af1(s/s):                    -0.3637978807E-011
week:                         1333

******** Week  309 almanac for PRN-27 ********
ID:                           27
Health:                       000
Eccentricity:                 0.1910161972E-001
Time of Applicability(s):  589824.0000
Orbital Inclination(rad):     0.9546477765
Rate of Right Ascen(r/s):  -0.7771752296E-008
SQRT(A)  (m 1/2):             5153.715820
Right Ascen at Week(rad):     0.2616728169E+001
Argument of Perigee(rad):  -2.025655336
Mean Anom(rad):               0.1489402467E+001
Af0(s):                       0.9536743164E-005
Af1(s/s):                     0.0000000000E+000
week:                         1333

******** Week  309 almanac for PRN-28 ********
ID:                           28
Health:                       000
Eccentricity:                 0.1033115387E-001
Time of Applicability(s):  589824.0000
Orbital Inclination(rad):     0.9598009932
Rate of Right Ascen(r/s):  -0.7783181344E-008
SQRT(A)  (m 1/2):             5153.591309
Right Ascen at Week(rad):  -0.2545444876E+001
Argument of Perigee(rad):  -2.310767162
Mean Anom(rad):               0.1708935491E+000
Af0(s):                       0.4386901855E-004
Af1(s/s):                     0.0000000000E+000
week:                         1333

******** Week  309 almanac for PRN-29 ********
ID:                           29
Health:                       000
Eccentricity:                 0.8738517761E-002
Time of Applicability(s):  589824.0000
Orbital Inclination(rad):     0.9836915455
Rate of Right Ascen(r/s):  -0.7771752296E-008
SQRT(A)  (m 1/2):             5153.600586
Right Ascen at Week(rad):     0.1613829431E+001
Argument of Perigee(rad):  -1.090825872
Mean Anom(rad):              -0.1579502117E+000
Af0(s):                       0.2193450928E-003
Af1(s/s):                     0.2546585165E-010
week:                         1333

******** Week  309 almanac for PRN-30 ********
ID:                           30
Health:                       000
Eccentricity:                 0.8232116699E-002
Time of Applicability(s):  589824.0000
Orbital Inclination(rad):     0.9438380056
Rate of Right Ascen(r/s):  -0.7966046104E-008
SQRT(A)  (m 1/2):             5153.604492
Right Ascen at Week(rad):  -0.2594338641E+001
Argument of Perigee(rad):     1.267049031
Mean Anom(rad):               0.4680304214E+000
Af0(s):                       0.3204345703E-003
Af1(s/s):                     0.1818989404E-010
week:                         1333

******** Week  309 almanac for PRN-31 ********
ID:                           31
Health:                       063
Eccentricity:                 0.1193428040E-001
Time of Applicability(s):  589824.0000
Orbital Inclination(rad):     0.9349576949
Rate of Right Ascen(r/s):  -0.8011762293E-008
SQRT(A)  (m 1/2):             5153.600098
Right Ascen at Week(rad):  -0.1570024468E+001
Argument of Perigee(rad):     1.135752484
Mean Anom(rad):               0.2155630247E+001
Af0(s):                       0.8583068848E-005
Af1(s/s):                     0.3637978807E-011
week:                         1333
```